M 2022

U.PORTO
FEUP FACULDADE DE ENGENHARIA
UNIVERSIDADE DO PORTO

THERMAL SWING ADSORPTION TECHNOLOGY DEVELOPMENT FOR VOCS AND SILOXANES REMOVAL

ANA MARGARIDA REBELO FARIA BAPTISTA

MASTER THESIS IN CHEMICAL ENGINEERING

PRESENTED TO THE FACULTY OF ENGINEERING OF THE UNIVERSITY OF PORTO

Master in Chemical Engineering

Thermal Swing Adsorption technology development for VOCs and siloxanes removal

Master dissertation

of

Ana Margarida Rebelo Faria Baptista

Developed within the course of dissertation

held in

DMT Environmental Technology

Supervisor: Prof. Alexandre Ferreira

Coordinator at DMT: Jort Langerak

U.PORTO
FEUP FACULDADE DE ENGENHARIA UNIVERSIDADE DO PORTO

DEPARTAMENTO DE ENGENHARIA QUÍMICA

July 2022

The work presented in this dissertation was performed at
DMT Environmental Technology
Joure, Netherlands.

Ana Margarida Rebelo Faria Baptista
E-mail: up201706792@fe.up.pt
E-mail: a.m.r.f.baptista@gmail.com

Faculdade de Engenharia da Universidade do Porto
Departamento de Engenharia Química
Rua Dr. Roberto Frias s/n
4200-465 Porto
Portugal

This document was typeset with LaTeX

Acknowledgements

I would like to express my gratitude to:

- DMT Environmental Technology for taking me for a dissertation within an internship, its employees for the best reception that can be provided. Major gratitude goes towards my company supervisor Jort Langerak, for being available to answer all my questions and guiding me through this project.

- Professor Alexandre Ferreira, for his role as supervisor at FEUP, enabling this dissertation to take place. Thank you for the guidance, support, and the encouraging words.

- My course friends, Beatriz and Sofia. Thank you for all the moments we spent together throughout the half a decade in FEUP. All the deep talks, support, and laughs; five years later, and it is ∴. I also want to extend my gratitude to my friends Gil, Manuel, and Rita, whom FEUP allowed me to meet, making the FFNC group complete. Thank you for all the gatherings, nights out, random stories, and mainly for the unconditional support.

- A special thank you for all of my friends that were always there for me and with whom I spent the best times and created the best memories. Without you it would definitely not be the same.

- Erasmus-Estágio program that enabled this internship to happen, just like Erasmus + did for my time in Belgium (Leuven) on the last semester. Both have contributed significantly to extending my professional and personal horizons. A special thank you goes to my Leuven friends for the most memorable semester. I would also like to extend my gratitude to Miguel and Daniela, with whom I spent the last 5 months in Joure. Also, thank you to Ana with Stasia for being a fantastic friend, giving us support, and unforgettable moments.

- To both of my parents, the most important and influential people in my life, for teaching me to become who I am and for always supporting me to get where I am now. Outstanding remarks to my brother António for being the best older irmãozinho and the best example I could follow. Thank you for your consistent support, compassion, and encouragement to be the greatest version of myself.

- To my grandparents Avô Baptista e Avó Lulu, who unfortunately could not see me graduate but considerably contributed to my education. I will keep you in a very special place, always.

With sincere appreciation,

Ana Margarida Rebelo Faria Baptista

Professor Alexandre Ferreira, supervisor of this dissertation is a member of LSRE-LCM - Laboratory of Separation and Reaction Engineering – Laboratory of Catalysis and Materials, financially supported by LA/P/0045/2020 (ALiCE), UIDB/50020/2020 and UIDP/50020/2020 (LSRE-LCM), funded by national funds through FCT/MCTES (PIDDAC).

Abstract

Global energy demand is increasing, and fulfilling this necessity with renewable sources over fossil fuels is imperative. Biogas (BG) is a renewable energy source that combines the use of biological waste with the ability to reduce greenhouse gas emissions. Microorganisms produce BG in anaerobic conditions, being mainly composed of carbon dioxide, methane, ammonia, nitrogen and trace components. Methane is the valuable compound of this stream; therefore, treatment is required for its purification. This work will mainly focus on removing Volatile Organic Compounds (VOCs) and siloxanes that partially compose the trace components group.

DMT features *Carborex MS* technology that combines a pre-processing unit followed by a membrane upgrading step. Removing VOCs and siloxanes in the first stage is critical to maintaining membrane efficiency and lifetime. For the removal of these compounds, carbon filters are used without a regenerative step which implies high replacement costs for this technology. Adsorption methods have been seen as viable alternatives, particularly Thermal Swing Adsorption (TSA), which is a cost-effective and robust technique, usually with two or more similar columns for inlet flow interchange. This technique uses the difference in temperature to change the adsorption equilibrium, allowing the impurities to adsorb at lower temperatures and desorb while increasing the temperature.

In this work, a 3-step TSA model was implemented in *Aspen Adsorption* to purify 1800 $nm^3\,h^{-1}$ of biogas. Each cycle comprises an adsorption step followed by the heating and cooling steps that operated in counter current. For a configuration of three and two columns, a recovery of the impurities in the waste stream of 95 % and 98 %, was achieved respectively.

From the obtained results, it was possible to conclude that regeneration optimization is required, either by increasing the temperature or the purge flow rate, to achieve 100 % removal and the consequent 100 % VOC/siloxane recovery in the waste stream. The regeneration step presents a vital role in the decrease of the safety factor of the column rather than the cooling time, however, an increase of the temperature in the light product stream is expected during adsorption and might influence the membranes stage. Finally, a parametric analysis was conducted to determine the effect of various parameters on TSA performance. It was concluded that lowering the regeneration temperature influenced mostly the waste stream recovery and increasing the purge flow would primarily affect the column safety factor. The inlet velocity and column length variation showed that lowering both parameters improved the regeneration efficiency.

Keywords: Biogas pre-treatment; Temperature Swing Adsorption; Regeneration; Activated carbon; Aspen Adsorption

Resumo

A crescente necessidade global de energia de fontes renováveis em detrimento dos combustíveis fósseis. O biogás é uma fonte de energia renovável que combina o uso de resíduos biológicos com a capacidade de reduzir as emissões de gases de efeito estufa. Este gás provém da atividade anaeróbica de microorganismos, sendo constituído por dióxido de carbono, metano e outros componentes presentes em baixas concentrações. O metano é o composto valioso desta corrente; portanto, é necessário um tratamento para sua purificação. Este trabalho irá ser focado principalmente na remoção de compostos orgânicos Voláteis (VOCs) e siloxanos, que compõem parcialmente o grupo de componentes de menores concentrações.

A DMT possui a tecnologia *Carborex MS*, que combina uma unidade de pré-tratamento seguida de uma etapa de membranas de aprimoramento. A remoção de VOCs e siloxanos no primeiro estágio é fundamental para manter a eficiência e a vida útil das membranas. Para a remoção destes compostos, são utilizados filtros de carvão sem uma etapa de regeneração, implicando altos custos de reposição para esta tecnologia. Os métodos de adsorção têm sido vistos como alternativas viáveis, particularmente a adsorção por TSA, que é uma tecnologia económica e robusta, geralmente associada a duas ou mais colunas semelhantes para troca de caudal de tratamento. Esta técnica usa a diferença de temperatura para alterar o equilíbrio de adsorção, permitindo que as impurezas sejam adsorvidas em temperaturas mais baixas e dessorvidas aquando do aumento da temperatura.

Neste trabalho, um modelo TSA de 3 etapas foi implementado no *Aspen Adsorption* para a purificação de $1800\,\mathrm{nm^3\,h^{-1}}$ de biogás. Cada ciclo compreende uma etapa de adsorção seguida das etapas de aquecimento e arrefecimento, que operam em contracorrente. Para a configuração de duas e três colunas, obteve-se a recuperação das impurezas na corrente pesada de 98 % e 95 %, respectivamente.

A partir dos resultados obtidos, foi possível concluir que a otimização da regeneração é necessária, seja aumentando a temperatura ou o caudal de purga, para atingir 100 % de remoção e consequente 100 % de recuperação de VOCs e siloxanos na corrente pesada. A etapa de regeneração apresenta um papel importante na diminuição do fator de segurança da coluna ao invés do tempo de arrefecimento, no entanto, um aumento da temperatura na corrente de produto leve é esperado durante a adsorção, podendo influenciar o desempenho das membranas. Finalmente, uma análise paramétrica foi realizada para determinar o efeito de vários parâmetros no desempenho do TSA. Concluiu-se que a redução da temperatura de regeneração influenciou principalmente a recuperação no fluxo de resíduos, e o aumento do fluxo de purga influencionou nomedamente o fator de segurança da coluna. A variação da velocidade de entrada e do comprimento da coluna mostrou que a redução de ambos os parâmetros melhorou a eficiência da regeneração.

Palavras-chave: Pré-tratamento do biogás; Temperature Swing Adsorption; Regeneração; Carvão ativado; Aspen Adsorption

Declaration

I hereby declare, under word of honour, that this work is original and that all non-original contributions is indicated and due reference is given to the author and source

July 4, 2022

Index

List of Figures

List of Tables

Notation and Glossary

a_p	Specific surface area	m^{-1}
b_0	Adsorption constant	$\mathrm{bar}^{-\mathrm{t}}$
C	Concentration	$\mathrm{mol\ m}^{-3}$
C_ps	Solid heat capacity	$\mathrm{J\ kg}^{-1}\ \mathrm{K}^{-1}$
C_vg	Fluid heat capacity	$\mathrm{J\ kg}^{-1}\ \mathrm{K}^{-1}$
D_ax	Axial dispersion coefficient	$\mathrm{m}^2\ \mathrm{s}^{-1}$
D_b	Bed diameter	m
D_h	Effective diffusivity	$\mathrm{m}^2\ \mathrm{s}^{-1}$
D_K	Knudsen diffusivity	$\mathrm{m}^2\ \mathrm{s}^{-1}$
D_M	Molecular diffusivity	$\mathrm{m}^2\ \mathrm{s}^{-1}$
D_p	Pores diffusivity	$\mathrm{m}^2\ \mathrm{s}^{-1}$
D_v	Volume diffusion	-
F	Flowrate	$\mathrm{mol\ h}^{-1}$
h_f	Heat transfer coefficient	$\mathrm{W\ m}^{-2}\ \mathrm{K}^{-1}$
k_LDF	Mass transfer coefficient	s^{-1}
k_s	Geometrical factor	-
L	Bed height	m
M_W	Molecular weight	$\mathrm{g\ mol}^{-1}$
p	Partial pressure	bar
P	Pressure	bar
P_u	Purge flow	$\mathrm{mol\ h}^{-1}$
q	Adsorption capacity	$\mathrm{mol\ kg}^{-1}$
R	Gas constant	$\mathrm{J\ mol}^{-1}\ \mathrm{K}^{-1}$
r	Radius	m
T	Temperature	K
t	Langmuir-Freudlich parameter	-
u_0	Superficial velocity	$\mathrm{m\ s}^{-1}$
u_i	Interstitial velocity	$\mathrm{m\ s}^{-1}$
y	Molar fraction	$\mathrm{kmol\ kmol}^{-1}$

Greek letter

ε	Porosity	-
ρ	Density	kg m^{-3}
μ	Viscosity	N s m^{-2}
τ	Tortuosity	-
λ	Thermal conductivity	W m^{-1} K^{-1}
Ω	Linear driving force factor	-
ΔH	Isosteric heat of adsorption	J mol^{-1}

Indexes

$*$	Equilibrium
ads	Adsorption
b	Packed bed
des	Desorption
exp	Experimental
f	Fluid
g	Gas
i	Component
mod	Model
p	Particle
reg	Regeneration
s	Solid
sat	Saturation
t	Total

List of acronyms

AC	Activated Carbon
BG	Biogas
CSS	Cycle Steady-State
HPR	Hypercrossedlinked
MC	Multi Component
MOFs	Metal Organic Frameworks
MTC	Mass Transfer Coefficient
PSA	Pressure Swing Adsorption
SC	Single Component
SS	Sum of Squares
TSA	Thermal Swing Adsorption
VOCs	Volatile Organic Compounds
VSA	Vacuum Swing Adsorption

Chapter 1

Introduction

1.1 Framing and presentation of the work

Global energy demand is growing rapidly, and fulfilling this necessity is challenging. As the majority part of the energy is produced by fossil fuels, vast amounts of greenhouse gases are released every day, becoming one of the increasing factors of global warming. Furthermore, because most known oil and gas deposits are located in politically unstable locations, there is a global concern relating to energy supplier security.

With this in mind, it is urgent to find alternatives to the traditional energy sources, and the solution relies on renewable ones. Biogas (BG) is a renewable energy source that combines the utilization of the organic waste produced by modern societies and the capability to decrease greenhouse gas emissions [1].

BG is produced under anaerobic conditions, where a population of microorganisms decomposes the organic waste into different compounds. It can be made in various environments such as landfills, sewage sludge, and biowaste digesters [2]. The BG produced in landfills typically has the following composition: 45-55 % of methane, 30-40 % of carbon dioxide, and 5-15 % of nitrogen [2]. Other components are also present in lower concentrations, such as hydrogen sulfide, ammonia, water, siloxanes, and Volatile Organic Compounds (VOCs). Their composition will vary depending on the feedstock.

Methane is a valuable energetic compound mainly used as biofuel for vehicles or heat and electricity generation [1]. Compounds like CO_2, N_2, and trace components are considered impurities, as they decrease the specific heat of biomethane. An upgrading step needs to be done to the BG streams to remove these components, therefore, meeting the required concentration specifications for its final applications. The pre-treatment stage comes before this phase to reduce trace components concentration. This is a pivotal step, as these compounds have harmful environmental impacts and reduce the upgrading system efficiency, even though they are present in lower concentrations.

The presented work will be focused mainly on the elimination of VOCs and siloxanes. Previous research on absorption strategies for the elimination of these compounds was conducted. Even though these approaches demonstrated significant removal efficiency, the solvent recovery stage increased energy costs, making this process uneconomical.

Adsorption methods have been seen as alternatives, particularly Thermal Swing Adsorption (TSA). TSA is regarded as a cost-effective and robust removal technology, and its VOCs and siloxanes removal performance will be studied in detail in this work.

As shown in Figure 1.1, the adsorption column will operate in a pre-treatment unit downstream of the desulphurization and water removal steps.

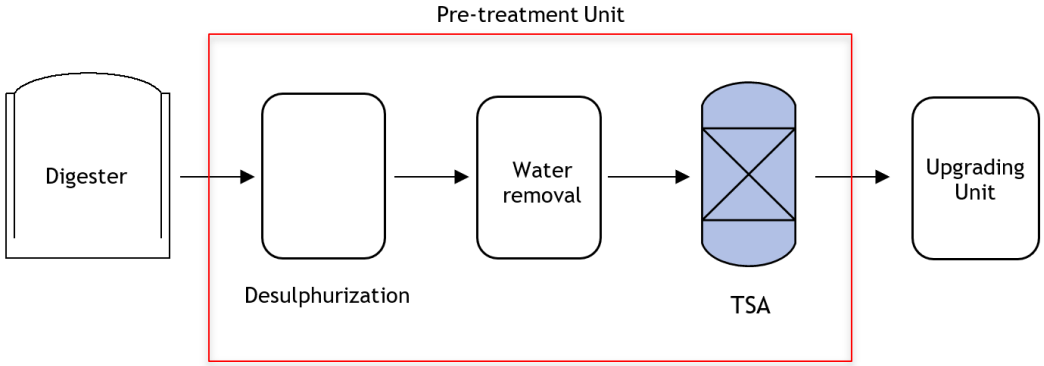

Figure 1.1: Biogas treatment scheme.

1.2 Presentation of the company

DMT was founded in 1987 and has since developed technologies to handle environmental challenges. The last ten years have been focused on biogas upgrading. Different products were designed: *Carborex MS*, which is a multi-stage membrane technology for biogas upgrading, and *Sulfurex* for biogas desulphurization.

Nowadays, DMT has offices in Europe, Asia, Canada, and the United States of America, and its headquarters is located in the Netherlands, more specifically in Joure. DMT currently employs around 70 people, and Theo Zuijdwijk has led this company, as CEO, since 2021.

1.3 Contribution of the author to the work

To find equilibrium data for the various components in the carbon media, a literature research was conducted. In this sense, adsorption equilibrium data for several compounds was gathered and delivered to the company in the form of a report.

Working with *Aspen Adsorption* required extra effort and dedication, since in the first stage, there was a lack of working experience with this software. However, some trials, tutorial guides and intensive software study was done allowing the achievement of the presented results. A TSA model was then implemented, being an useful tool for following up tasks.

Indeed, all the work presented in this manuscript was performed by the author, and itself was a represented in a significant advancement for the DMT know-how on TSA and its application on low concentration components removal by adsorption based processes.

1.4 Organization of the dissertation

This work is organized in six different chapters. The detailed information of each chapter is presented as follows:

- Chapter 1 - Introduction: presents the framework of the project, presents the company and states the main contribution of the author over the present work
- Chapter 2 - State of the art: outlines which strategies have been investigated for biogas cleaning; presents an analytical perspective of adsorption technologies more specifically of TSA for siloxanes, and VOCs removal.
- Chapter 3 - Materials and methods: a description of the theoretical equations and models used in the Aspen Adsorption program as the inputs specifications for the simulations.
- Chapter 4 - Results and discussion: obtained results for single and multi component adsorption in a three column system and multi component adsorption for a two column system; time-step optimization for both configurations; parametric study.
- Chapter 5 - Conclusions: presents the main conclusions from the obtained data and summarizes the main goals achieved.
- Chapter 6 - Assessment of the work done: the achieved objectives, limitations, and future work that can be done from this project are all specified.

Chapter 2

State of the art

2.1 VOCs and siloxanes removal

Volatile organic compounds are pollutants generated by chemical, pharmaceutical, food and electronic material industries, among others. VOCs are defined by the World Health Organization as organic compounds having a saturated vapor pressure more than 133 Pa and a boiling point range from 50 °C to 260 °C at atmospheric pressure [3]. These compounds can be classified according to their molecular structure and it includes alkanes, alkenes, aromatic hydrocarbons, alcohols, aldehydes, terpenes and ketones, among others. For VOCs abatement, a wide range of post-processing technologies have been developed, which may be divided into two categories: destruction technology and recovery technology. Destructive methods decompose the VOCs into other compounds, whereas recovery methods separate these components from the integrated system by changing the operation conditions of the process [4]. The operating cost, the removal efficiency as the tolerable feed concentration of the pollutants are compared in Table 2.1.

Table 2.1: VOCs control techniques comparison [4; 5].

Techniques	**Annual operating cost (€/cfm)**	**Removal efficiency (%)**	**Pollutant concentration (ppm)**
Thermal oxidation	$13-132$	$95-99$	$100-1000$
Catalytic oxidation	$13-80$	$90-98$	$100-1000$
Absorption	$22-106$	$90-98$	$500-15000$
Adsorption	$9-31$	>95	$700-10000$
Condensation	$18-106$	$70-85$	>5000
Membranes	$13-26$	$90-99$	$2000-50000$

Siloxanes can be described as subgroups of silicone containing Si-O bonds with organic radicals bonded to Si. They are found in products like oils which are used in cosmetic products, foam inhibitors, cleaning products, excipients in medicines and food additives, among others [6]. During the combustion

of biogas, siloxanes are converted into silicon dioxide deposits, leading to abrasion of engine parts, inhibiting heat conduction [7]. The removal of these compounds can be achieved while performing adsorption in a fixed and fluidized bed, absorption, and gas chilling methods.

DMT presents a technology, *Carborex MS*, that enables the production of biomethane with high purity, depending on the end-use requirements. It combines a pre-processing step and a membrane upgrading configuration. VOCs and siloxanes removal are pivotal points in maintaining membranes efficiency and lifetime. An activated carbon bed is part of the pre-treatment step in this technology, particularly in the VOCs and siloxanes removal. Significant removal efficiencies can be obtained with this adsorbent, however, for higher contents, activated carbon might not be efficient. As it also does not include a regenerative stage, high replacement costs are coupled with this technique.

Alternative methods have been investigated to reduce operating costs while maintaining removal efficiency. Some projects were previously developed [8; 9] where the absorption methods were studied for the removal of this trace components. The absorption approach, that consisted in a scrubber, was considered with a combination of water and selexol as solvent. It was shown in these studies, that a high removal effectiveness was obtained. However, the solvent recovery stage would require increased energy expenses.

As indicated in Table 2.1, adsorption techniques are related with reduced operational expenditures; moreover, it is regarded as one of the most promising VOCs treatment technologies due to its cost-effectiveness, flexibility, and low energy usage [4].

2.2 Adsorption technologies

Adsorption is an exothermal surface phenomenon that involves the transfer of a molecule from a fluid bulk to a solid surface. It involves two different stages, the diffusion of a component from the bulk into the pores of the solid and the binding of that component inside a pore [10]. Yet, the driving force for the migration of the chemical species is the difference in chemical potential.

Gas separation can be achieved by one of the three mechanisms: steric, kinetic, or equilibrium effect. The steric effect derives from the molecular sieving property. Kinetic separation is achieved by the molecules diffusion rate difference. The majority of processes operate through the equilibrium adsorption of the mixture.

The interaction between the solid and bulk phase will dictate the type of adsorption, as it can be physisorption (reversible phenomenon) or chemisorption. When a molecule comes into contact with the adsorbent surface, it experiences a decrease in its potential energy, which is known as Lennard-Jones, being this the cause of adsorption. When the pores walls are relatively far from the adsorbate which usually happens on the macropores ($\oslash > 50\,\text{nm}$) and the mesopores ($50\,\text{nm} > \oslash > 2\,\text{nm}$), the molecule can travel through it in its free state via knudesen diffusion. However, when a molecule reaches the micropores ($\oslash < 2\,\text{nm}$), the distance is so small that the molecule enters in a potential well, then the compound moves through a superficial phenomena. In physical adsorption, the adsorption is based on the dispersive forces of Van der Waals that is associated with a lower heat of adsorption. Other

forces can be associated, like hydrogen bonding, permanent dipole/ permanent dipole or permanent dipole/ induced dipole, that are associated with a higher heat of adsorption [11].

Depending on the operating procedures, the separation can be classified as Thermal Swing Adsorption, Pressure Swing Adsorption (PSA), and Vacuum Swing Adsorption (VSA). These are the most prevalent strategies, but they can be combined depending in some circumstances on the pretended end product.

When the solid achieves its maximum adsorption capacity, regeneration occurs, allowing the trapped compounds to be released. It is accomplished by increasing the operating temperature of the adsorbent when operating with a TSA mode or decreasing the pressure while working with a PSA or VSA mode. These methods were compared with the VOCs and siloxanes removal in perspective, and it is presented in table 2.2.

Table 2.2: Comparison of different adsorption technologies [12; 13].

Techniques	**Advantages**	**Disadvantages**
PSA	Rapid Regeneration	Higher operating costs related to the compressor acquisition
TSA	Simple and more economic More effective for VOCs and Siloxanes removal	Requires a time-consuming cooling and heating steps Not Suitable for sensitive and readily polymeriable compounds
VSA	Less energy consumption compared to the PSA	Higher operating costs related to the vacuum Lower efficiency on the VOCs' regeneration

Within the mentioned adsorption methods, TSA shows itself as a efficient technique, being a cost-effective and robust removal technology [14]. Hence, Temperature Swing Adsorption technology will be studied in greater depth during this work with the primary goal of removing VOCs and siloxanes.

2.3 Temperature Swing Adsorption

TSA works with the difference in temperature for streams treatment. As adsorption is an exothermal phenomenon, lower temperatures will favour the equilibrium in this step, meaning that a higher quantity of compounds is adsorbed. On the other hand, higher temperatures will reverse the direction of the equilibrium. Thus the desorption of the adsorbate will occur.

The adsorption equilibrium between the adsorbent and the adsorbate is characterized by an isotherm. At a constant temperature, the adsorption equilibrium isotherm quantifies the amount of adsorbed compounds per mass or volume of the adsorbent as a function of the total species present in the gaseous phase.

Figure 2.1 depicts a temperature swing operating scheme. A larger amount of adsorbed gas is achieved at a lower temperature (T_{ads}). When a higher temperature (T_{des}) is set, the equilibrium is therefore described by a different isotherm, with a lower adsorption capacity.

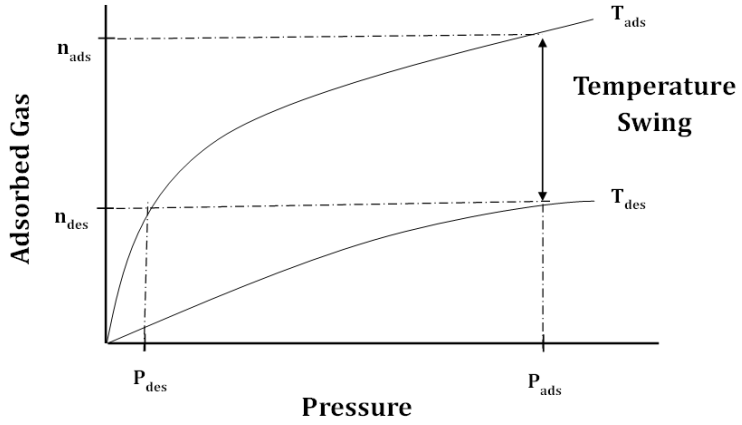

Figure 2.1: TSA isotherms operation scheme.

Vapor-phase adsorption processes for removing impurities frequently utilize a TSA cycle that follows three consecutive steps: adsorption, desorption, and cooling. In the first stage, the inlet gas flows through the column at ambient temperature, where the VOCs and siloxanes are adsorbed. In the second step, a hot purge gas flows in counter-current through the bed, volatilizing the retained compounds. The cooling stage lowers the temperature of the adsorbate and thereby "activates" it, making it ready for the next cycle to begin. These three mentioned steps are illustrated in Figure 2.2.

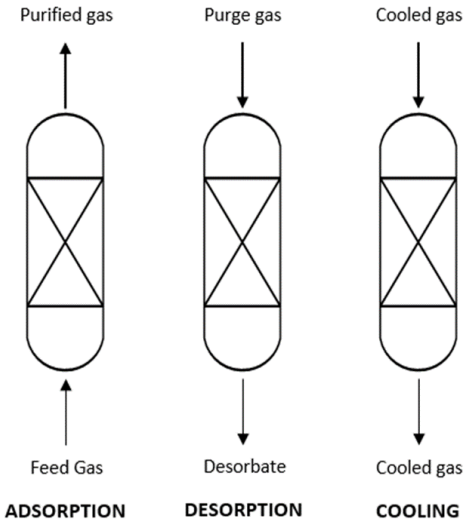

Figure 2.2: TSA three-step configuration.

The cooling and heating needs impact the TSA's overall performance and costs. As a result, one

of the essential influencing factors is heat transfer, requiring high transfer rates between the adsorbent and internal heat exchanger surfaces.

In industry, a TSA cycle can occur in two or three different packed beds. For the two-column system, while the first column is on the adsorption step, the second one is regenerated and cooled afterwards. The feed flow swaps position when the adsorbent achieves saturation and the second column has cooled down.

Regarding the three-column configuration, while the first column is adsorbing the impurities, the second one is being regenerated and the third one cooled down to the adsorption temperature. The feed flow swaps position when the adsorbent achieves saturation on the first column, and the third column has cooled down while the second one completed the regeneration step. Thus, column 3 will take the place of column 1, column 2 will replace column 3, and column 1 will replace column 2. When another clockwise rotation of the setup is complete, a new cycle is ready for operation.

Thermal regeneration has historically used steam to increase adsorbent temperature. However, other alternative heat sources were used, such as Joule effect, microwaves, embedded heaters, and heated nitrogen [15]. Several post-treatments are available for the purge gas, such as regenerative thermal oxidizers, vent air burners, flares, or diluters within the atmosphere with air.

2.3.1 Adsorbents

Choosing the correct adsorbent is one of the most challenging and critical aspects of adsorption separation technology. It will affect the efficiency, investment, and operating costs of the process.

The adsorption capacity will dictate the quantity of adsorbate captured per unit of mass or volume of adsorbent. This capacity raises as the specific surface area, pore-volume, and surface chemical functional groups increase, or the pore size decreases [16].

Activated carbon, zeolite, and hypercrossedlinked polymeric resins will be analyzed in more detail as they are listed as the three main adsorbents for VOCs control by the United States environmental protection agency. Metal organic frameworks (MOFs) materials will also be discussed as they present a large specific surface area and a rich surface chemical functional group [16]. These adsorbents can also be applied for siloxanes capture.

2.3.1.1 Activated carbon

Activated carbon (AC) is the most widely applied adsorption material because of its good physical and chemical properties (large specific surface area, abundant functional groups, chemical stability, high mechanical strength, and acid and alkali resistance). Activated carbons are produced by carbonization (using precursors like coconut shell, walnut shell, wood, resin, or coal) and activation (using activators like steam, CO_2, KOH, NaOH, among others) [16] . The specific surface area of the adsorbent will be influenced by the type of precursor, activator used, and the pore structure. The last can be adjusted controlling the production steps of the carbon.

This adsorbent has a higher affinity for compounds with a higher molecular weight and lower vapor pressure (higher boiling point) [17] . It can exhibit some disadvantages while operating with higher

temperatures, as it might ignite. Furthermore, the carbon removal efficiency decreases when moisture levels rise due to adsorption competition with the VOCs.

Other carbon-based adsorbents include activated carbon fibers, carbon nanotubes, and carbon silica composites, among others, and all of them can also be used for the same purpose. Because of the fiber structure and narrow and straight micropores, the carbon fibers present a quicker interparticle adsorption kinetics than AC. However, they have a poor performance when it comes to polar VOCs. Although carbon nanotubes are a promising VOCs adsorbent, aggregation is one of the most significant limitations that restricts their commercial usage. Carbon silica composites outperform AC because of their shorter diffusional route, greater affinity, lower mass transfer resistance, and higher ignition temperature [18].

2.3.1.2 Zeolites

Zeolites are crystalline aluminosilicates and are made up of a three-dimensional (3D) arrangement of TO_4 tetrahedrons (where T can be Al or Si). The zeolite Si content is related to its water resistance, which may be modified throughout the production process [4].

This type of adsorbents are widely used in environmental protection applications such as adsorption of VOCs and heavy metal ions due to its adjustable pore size, thermal stability, and ease of surface modification [16].

Compared with other adsorption materials, zeolites have a smaller specific surface area (250-800 $m^2\,g^{-1}$) and poorer VOCs adsorption capacity. However, it can be modified to have uniform and controlled micropores and customized wettability, increasing the selective adsorption of VOCs.

All naturally occurring zeolites are hydrophilic, having a higher attraction for polar substances like water. However, synthesized zeolite can be either hydrophilic or hydrophobic.

The superior hydrothermal and chemical stability of zeolites enable it to overcome the flammability and regeneration drawbacks that AC may present. However the synthesis process of zeolite is complex and time-consuming. Furthermore, the raw materials, such as tetraethyl orthosilicate and cetyltrimethyl ammonium bromide, are more costly than AC [4].

The removal of n-hexane while using zeolites was studied on zeolites with a surface area of $638\,m^2\,g^{-1}$ [19] and $750\,m^2\,g^{-1}$ [20]. Also, some experiments were made for acetone and toluene on zeolites with a surface area of $704\,m^2\,g^{-1}$ [21].

2.3.1.3 Hypercrosslinked polymeric resins

Polymeric adsorbents have emerged as a viable alternative to activated carbon for extracting organic contaminants from the aqueous solution because of their adjustable pore shape, chemical characteristics, and on-site regeneration [22].

Organic polymers can be divided in two categories: hypercrosslinked polymer resins (HPR) and macroporous polymers. HPR represents a class of microporous organic polymers that is low costing and synthesized by the Friedel-Crafts alkylation reaction. HPR is attributed to extensive crosslinking reactions and such nature confers them a high inner specific surface area (1000-1500 $m^2\,g^{-1}$).

Resins are usually based on co-polymers of styrene/divinylbenzene and acrylic acid esters/divinylbenzene for industrial uses. HPR are gaining more attention for VOCs removal due to their tailorable porosity, low weight, high thermal stability, and adaptability. Furthermore, due to the lack of surface chemical functional groups, HPR are hydrophobic under humid conditions, advantageous for moist gas streams. Complex synthesis processes are being developed in order to expand HPR popularization for large-scale applications [4].

Some studies were made on the preparation of a novel HPR for benzene removal with a HPR adsorbent exhibiting a surface area of $1244\,m^2\,g^{-1}$ [23] and $1345\,m^2\,g^{-1}$ [24]. Similarly, experiments were made for dicloromethane and 2-butanone removal with HPR [25].

2.3.1.4 Metal organic frameworks

Metal organic frameworks present a variety of organic and inorganic components in their structure, and they have emerged as a class of crystalline materials with ultrahigh porosity, internal surface area (up to $3000\,m^2\,g^{-1}$), thermal stability ($>400\,°C$), tailorable pore structure and facile functionalization [16; 4].

The structure of this type of adsorbents can be flexibly controlled while selecting matching organic ligands. Unlike other adsorbents, MOFs have the capacity to remain their structure and crystalline permanent after regeneration [4].

Different types of MOFs were compared for the toluene adsorption under ambient conditions, where a MOF with a surface area of $1401\,m^2\,g^{-1}$ [26] was used. Other type of MOF was used for the benzene removal, which had a surface area of $2080\,m^2\,g^{-1}$ [27]. A new modified MOF adsorbent was synthesized, reaching a specific area of $4293\,m^2\,g^{-1}$ [28].

These adsorbents are mainly used for laboratory experiments, however, some research is being made to up-scale it for industrial applications in a greener and cheaper way [16].

2.3.2 Adsorbent selection

Activated carbons are one of the most suitable adsorbents for the VOCs recovery. They present a large surface area, a high adsorption capacity, a non-selective nature, and low-cost pricing [29; 30]. With this in mind, and knowing that equilibrium data is mostly available in the literature for this type of adsorbent, a more extensive search for AC was conducted.

Adsorption equilibrium data was found for some carbon adsorbents, however four different ones were chosen, as they present more information for the VOCs. Appendix A compiles a table with the biogas composition from a DMT client and the respective concentration of the presented VOCs.

In order to understand which carbon would present data for a higher amount of VOCs, a score system was made for each adsorbent. If an isotherm in the literature was found for the component, a number "1" was given to it. A total VOCs concentration sum for each carbon was calculated, and it is possible to confirm that BPL carbon has the highest value. It is also important to mention that this carbon was already studied for two of the compounds with higher concentration on the biogas stream.

Consequently, BPL carbon was the chosen adsorbent to use for the TSA process. Figure 2.3 depicts the BPL carbon adsorption isotherms for a subset of VOCs which compose the flow stream. To simplify the graph display, only the isotherm with respect to 298 K temperature is represented.

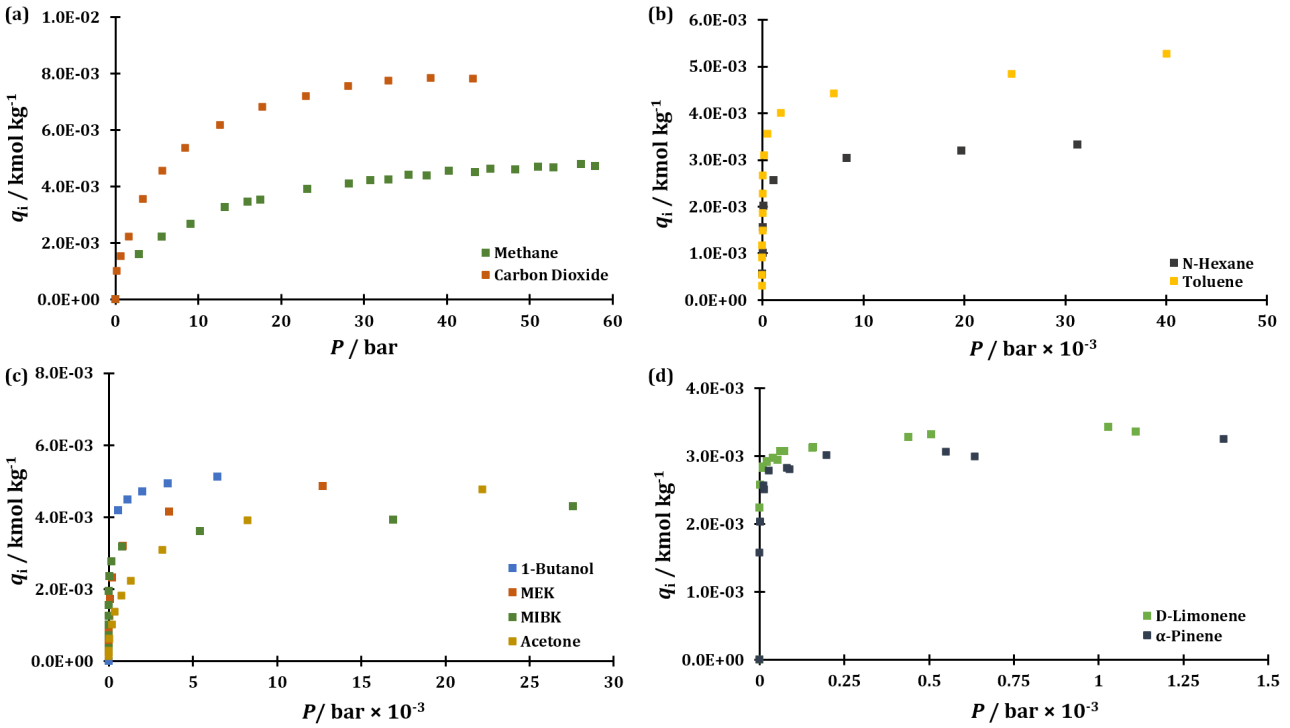

Figure 2.3: Adsorption isotherms measured in BPL at 298 K of (a) methane and carbon dioxide; (b) N-Hexane and toluene; (c) 1-Butanol, MEK, MIBK and Acetone; (d) D-Limonene and α-Pinene [31; 32; 33; 34; 35].

Chapter 3

Materials and methods

The software *Aspen Adsorption V12* was used as tool for the building and simulation of a TSA model for VOCs and siloxane's removal. Different steps were considered for the development of this project. In the first place, an adsorbent selection was made for the packed media. Afterwards, two different configurations of the TSA columns were considered: the three-column and two-column configuration scheme. To validate the performed model, a validation with field data available for a three-column scheme was made in the first place, considering only toluene as an impurity. After that, an upgrade of the system into multi component adsorption was made. Since there are some limitations on the running time simulations, the performed models only took into account the presence of 4 compounds besides carbon dioxide and methane. The component with the highest concentration in the biogas flow of each VOCs family was chosen in addiction of one siloxane. The alkanes were not considered as they are present at lower concentrations ($<0.2\,\text{ppm}$) and would unnecessarily lengthen the simulations. A more specific list with the considered components are present in Appendix B with the respective physical properties.

3.1 Adsorbent specification

As mentioned in Section 2.3.2, BPL carbon was found to be the adsorbent that was best suited for the simulations. More information can be found in table 3.1.

Table 3.1: BPL adsorbent physical properties [34; 36; 37; 38].

Property	**BPL (6x16)**
BET Surface area ($\text{m}^2\,\text{g}^{-1}$)	1150
Particle density ($\text{kg}\,\text{m}^{-3}$)	430
Particle radius (mm)	1
Average pore size (nm)	1
ε_b	0.40
ε_p	0.35
Specific heat capacity ($\text{J}\,\text{kg}^{-1}\text{K}^{-1}$)	1560

The carbon media used in this study was microporous BPL activated carbon (6x16 mesh) with a spherical shape, which can be supplied by Calgon Carbon Corp.

3.1.1 Isotherm

A fitting step was made to the experimental points from the isotherms found in the literature, in order to understand which isotherm would represent the data with a minimal error. Two different isotherm models were tested: Langmuir and Freundlich-Langmuir model. Appendix C summarizes the fitting test that was made to the experimental data to understand which model would represent it with more accuracy.

From the information reported in Appendix C, it is possible to understand that the model that confers a lower fitting error is the Langmuir-Freundlich model. Hence, the isotherm for the pure component was predicted by this model and the respective equation is expressed in equation 3.1:

$$q_{\mathrm{i}} = q_{\mathrm{i,sat}} \frac{\left(b_{0,\mathrm{i}} \mathrm{e}^{-\frac{\Delta \mathrm{H_i}}{RT}} p_{\mathrm{i}} \right)^t}{1 + \left(b_{0,\mathrm{i}} \mathrm{e}^{-\frac{\Delta \mathrm{H_i}}{RT}} p_{\mathrm{i}} \right)^t} \tag{3.1}$$

where q_{i} is the adsorption capacity, $q_{\mathrm{i,sat}}$ the maximum adsorption capacity for each component, $b_{0,\mathrm{i}}$ the adsorption constant, R the gas constant, T the operating temperature, p_{i} the partial pressure of each component, t the Langmuir-Freundlich parameter and ΔH_i the isosteric heat of adsorption of each component. The isosteric heat was computed using isotherms at different temperatures, except for the terpene, where only one temperature was available. In this case, a given value from the literature was taken into account.

Figure 3.1 depicts the fitted isotherm of each compound as Table 3.2 specifies the respective isotherm parameters. Due to a paucity of information in the literature regarding the adsorption of octamethylcyclotetrasiloxane (D4) on BPL carbon, an assumption was made about this compound's isotherm. This prediction was made based on an adsorption study of D4 in *PICABIOL* activated carbon [39]. Using both D4 and toluene isotherms for the reference carbon, a prediction was made to the BPL carbon, based on the ratio difference of each parameter.

Table 3.2: Parameters for the Freundlich-Langmuir model for each component.

Compounds	$\mathbf{q_{sat}}$ ($\mathbf{kmol\,kg^{-1}}$)	$\mathbf{b_0}$ ($\mathbf{bar^{-1}}$)	-ΔH ($\mathbf{J\,mol^{-1}}$)	**t**
Methane	6.35×10^{-3}	1.12×10^{-4}	16279	0.78
Carbon Dioxide	1.10×10^{-2}	7.04×10^{-6}	23972	0.72
D-Limonene	6.24×10^{-3}	5.17×10^{-5}	47000	0.08
1-Butanol	5.38×10^{-3}	9.98×10^{-7}	58601	0.50
D4	2.02×10^{-3}	2.12×10^{-2}	33120	0.26
Toluene	5.52×10^{-3}	1.88×10^{-5}	50085	0.33

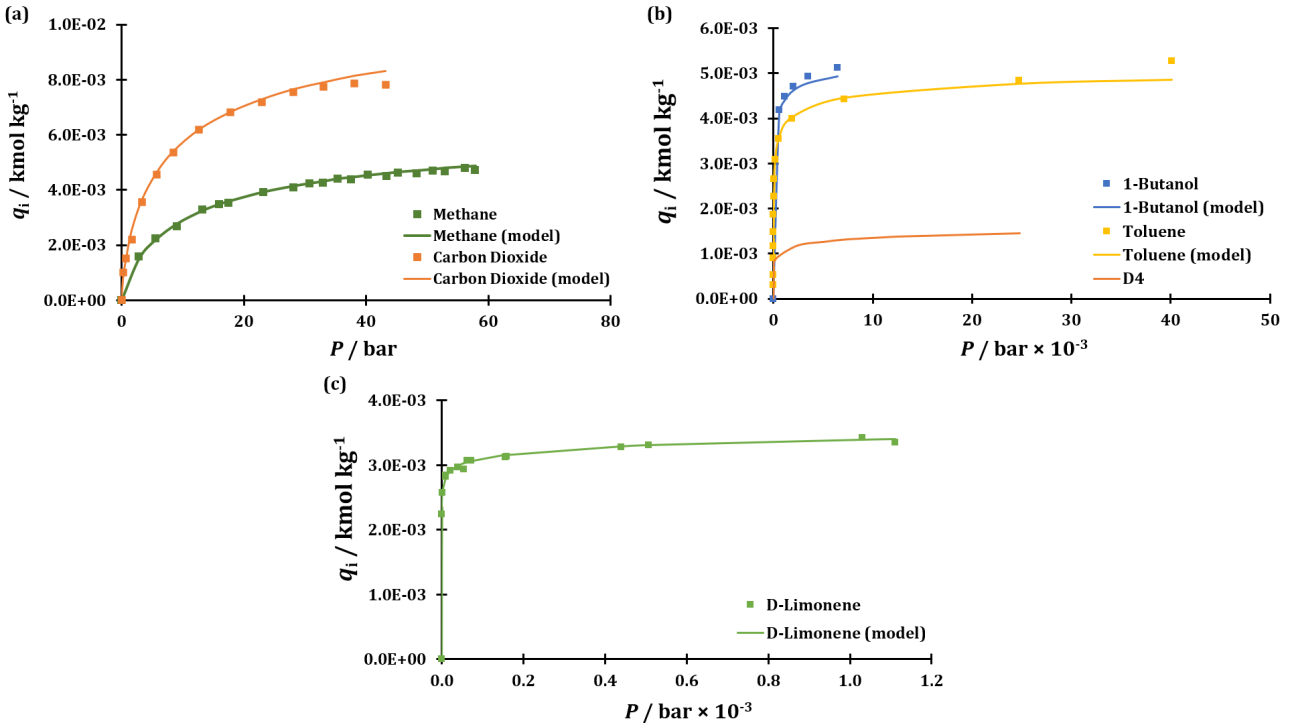

Figure 3.1: Adsorption isotherms in BPL at 298 K of (a) methane and carbon dioxide; (b) 1-Butanol, toluene and D4; (c) D-Limonene.

3.2 Aspen Adsorption configuration

The software that was used for the TSA simulation was *Aspen Adsorption V12*. For the performed model, the Gas Dynamic mode was selected. The flowsheet was composed by a Gas Bed, Gas Tank Voids, Gas Valves, Gas Feed stream and a Gas Product stream. These blocks were connected by Gas Material Connection streams.

The components list was specified in the first place with all the present components in the system. Afterwards, the thermodynamic model was specified. Since the VOCs and siloxanes' concentration is relatively low compared to the total flow composition, the ideal model was chosen.

Appendix D presents the aspen adsorption flowsheet that was used for the cycle simulation of the TSA.

Over the next sections the bed configuration will be specified as it is the core part of the model.

3.2.1 Adsorption bed configuration

A single layer bed of activated carbon was simulated as a vertical type, 1D spacial dimensions without an internal heat exchanger and it was divided in 20 different nodes. Upwind Differencing Scheme 1 (USD 1) was the chosen discretization method, being the one that shows a better accuracy and simulation time ratio.

3.2.1.1 Material balance

A material balance to the gas phase was done with the following assumptions: axial dispersion was considered while radial dispersion was neglected; mass convection was assumed with a constant value for dispersion; ideal gas behaviour was considered for the gas phase. The mass material balance is expressed in Equation 3.2:

$$\frac{\partial(C_{\mathrm{i}}u_0)}{\partial z}+\varepsilon_{\mathrm{t}}\frac{\partial C_{\mathrm{i}}}{\partial t}+(1-\varepsilon_{\mathrm{b}})\rho_{\mathrm{p}}\frac{\partial q_{\mathrm{i}}}{\partial t}+\varepsilon_{\mathrm{b}}D_{\mathrm{ax}}\frac{\partial^2 C_{\mathrm{i}}}{\partial z^2}=0 \tag{3.2}$$

where C_{i} is the gas phase concentration of the component i, u_0 the superficial velocity, ε_t the total porosity, ε_b the bulk porosity, ρ_p the particle density, q_{i} the adsorbed phase concentration and D_{ax} the axial dispersion coefficient.

3.2.1.2 Kinetic model

The adsorption of the components of the gas phase in the adsorbent shows some resistance on the mass transfer phenomena, due to the porous structure of the solid. The Lumped resistance assumption was selected for the kinetic model. This model considers that the individual mass transfer resistances are included as an overall component. This component has into account the resistance between the bulk gas phase and the gas-solid interface and the resistance related to the porous structure of the adsorbent. In order to describe the trajectory of the compounds from the bulk phase into the adsorbent, the linear driving force model was considered. In this model, the mass transfer driving force for component i is a linear function of the solid phase loading, and it is expressed by Equation 3.3:

$$\frac{\partial(q_{\mathrm{i}})}{\partial t}=k_{\mathrm{i,LDF}}(q_{\mathrm{i}}^{*}-q_{\mathrm{i}}) \tag{3.3}$$

where $k_{\mathrm{i,LDF}}$ is the Mass Transfer Coefficient (MTC) of each component, and q_{i}^{*} is the adsorbed phase concentration in equilibrium with gas phase. For the mass transfer coefficient calculation, the Glueckauf model approximation was performed for spherical particles [40], being expressed by Equation 3.4:

$$k_{\mathrm{i,LDF}}=\frac{\Omega D_{\mathrm{i,h}}}{r_{\mathrm{p}}^2} \tag{3.4}$$

where Ω represents the dimensionless linear driving force factor, $D_{\mathrm{i,h}}$ is the effective diffusivity constant of each component and r_{p} the particle radius. The dimensionless factor can be calculated with the correlation presented in Equation 3.5:

$$\Omega=(k_{\mathrm{s}}+1)(k_{\mathrm{s}}+3) \tag{3.5}$$

where k_{s} is the dimensionless geometrical factor for the solid, that takes a value of 2 due to the spherical geometry of the adsorbent.

3.2.1.3 Momentum balance

The Ergun's model was used to estimate the pressure drop along the bed and it is expressed in Equation 3.6:

$$-\frac{\partial P}{\partial z} = 150\frac{(1-\varepsilon_\mathrm{b})^2}{\varepsilon_\mathrm{b}^2}\frac{\mu_\mathrm{f}}{d_\mathrm{p}^2}u_0 + \frac{1-\varepsilon_\mathrm{b}}{\varepsilon_\mathrm{b}}\frac{\rho_\mathrm{f}}{d_\mathrm{p}}|u_0|u_0 \tag{3.6}$$

where μ_f is the viscosity of the fluid mixture and ρ_f the fluid density. It was showed that the Ergun equation can be used in modelling pressurization and blow down [41].

3.2.1.4 Energy balance

The energy balance represents the heat exchange in a non-isothermal bed where it was also considered solid and gas conduction. For simplification of the model, the column was considered adiabatic where it is assumed that the column is isolated. It was made an energy balance for the gas and solid phase that are expressed by equations 3.7 and 3.8, respectively. Firstly, for the gas phase, five terms are considered: axial thermal conduction, convection, thermal accumulation in the gas phase, heat transfer between the fluid and the adsorbent:

$$-\lambda_{\mathrm{ax,g}}\frac{\partial^2 T_\mathrm{g}}{\partial z^2} + \rho_\mathrm{g}\mathrm{u}_0 C_\mathrm{vg}\frac{\partial T_\mathrm{g}}{\partial z} + \rho_\mathrm{g}\varepsilon_\mathrm{t} C_\mathrm{vg}\frac{\partial T_\mathrm{g}}{\partial t} + (1-\varepsilon_\mathrm{b})a_\mathrm{p}h_\mathrm{f}(T_\mathrm{g}-T_\mathrm{s}) = 0 \tag{3.7}$$

where $\lambda_{\mathrm{ax,g}}$ represents the heat dispersion coefficient in the gas phase, T_g the gas temperature, ρ_g the gas density, $C_{\mathrm{v,g}}$ the fluid heat capacity, a_p the specific surface area of the adsorbent and h_f the heat transfer coefficients of the fluid/solid.

For the solid phase, five terms are considered: axial thermal conduction, thermal accumulation in the solid phase, thermal accumulation due to the heat release on the adsorption and heat transfer between the gas and the solid:

$$-\lambda_{\mathrm{ax,s}}\frac{\partial^2 T_\mathrm{s}}{\partial z^2} + \rho_\mathrm{p} C_\mathrm{ps}\frac{\partial T_\mathrm{s}}{\partial t} + (1-\varepsilon_\mathrm{b})a_\mathrm{p}h_\mathrm{f}(T_\mathrm{g}-T_\mathrm{s}) + \sum_{i=1}^{k}(-\Delta\mathrm{H_i})\frac{\partial q_\mathrm{i}}{\partial t} = 0 \tag{3.8}$$

where $\lambda_{\mathrm{ax,s}}$ represents the heat dispersion coefficient in the solid phase, C_ps the heat capacity T_s the solid temperature and $\Delta\mathrm{H_i}$ the isosteric heat of adsorption for each component.

3.2.1.5 Isotherm model

In order to represent a multicomponent adsorption, the Extended Langmuir-Freundlich model was selected in the model. The respective correlation is presented in Equation 3.9:

$$q_\mathrm{i} = q_{\mathrm{i,sat}}\frac{\left(b_{0,\mathrm{i}}\mathrm{e}^{-\frac{\Delta\mathrm{H_i}}{RT}}p_\mathrm{i}\right)^t}{1+\sum_{k=1}^{N}\left(b_{0,k}\mathrm{e}^{-\frac{\Delta\mathrm{H_k}}{RT}}p_\mathrm{k}\right)^t} \tag{3.9}$$

where q_i is the adsorption capacity, $q_{i,sat}$ the maximum adsorption capacity for each component, $b_{0,i}$ the adsorption constant, R the gas constant, T the operating temperature, p_i the partial pressure of each component, t the Langmuir-Freundlich parameter, ΔH_i the isosteric heat of adsorption and N the total number of components.

This model turns into the Freundlich isotherm at higher adsorbate concentrations, where it is assumed a multi-layer adsorption. The Langmuir isotherm model takes place at lower adsorbate concentrations, in which is assumed an adsorption occurring on a homogeneous surface. The parameter t of the equation can be considered as a parameter for assessment of adsorption sites heterogeneity. The higher the value of t, the lower level of surface heterogeneity is associated [42].

3.2.1.6 Bed layer specification

Input data for the bed layer is summarized in Table 3.3. Further information related to the isotherm parameters as the computation of other thermodynamic parameters is summarized in Appendix E. The mass transfer coefficients specification will be detailed in depth in the next chapter.

Table 3.3: Bed layer input parameters.

Parameter		Methane	Carbon dioxide	Limonene	Butanol	D4	Toluene
IP1	$kmol\,kg^{-1}$	6.35×10^{-3}	1.10×10^{-2}	6.24×10^{-3}	5.38×10^{-3}	2.02×10^{-3}	5.52×10^{-3}
IP2	bar^{-t}	8.00×10^{-4}	1.93×10^{-4}	4.55×10^{-1}	1.05×10^{-3}	3.72×10^{-1}	2.87×10^{-2}
IP3	-	7.84×10^{-1}	7.21×10^{-1}	7.98×10^{-2}	4.97×10^{-1}	2.57×10^{-1}	3.26×10^{-1}
IP4	K	1.53×10^{3}	2.08×10^{3}	4.51×10^{2}	3.50×10^{3}	1.02×10^{3}	1.97×10^{3}
IP5	bar^{-t}	8.00×10^{-4}	1.93×10^{-4}	4.55×10^{-1}	1.05×10^{-3}	3.72×10^{-1}	2.87×10^{-2}
IP6	K	1.53×10^{3}	2.08×10^{3}	4.51×10^{2}	3.50×10^{3}	1.02×10^{3}	1.97×10^{3}
E_z	$m^2\,s^{-1}$	6.00×10^{-5}					
L	m	4.40					
D_b	m	1.80					
HTC	$W\,m^{-2}\,K^{-1}$	408					
$\lambda_{ax,g}$	$W\,m^{-1}\,K^{-1}$	0.408					
$\lambda_{ax,s}$	$W\,m^{-1}\,K^{-1}$	555					

Chapter 4

Results and discussion

The performed simulations for the TSA were obtained based on the following model assumptions: ideal gas behavior; convection with axial dispersed plug flow; non-isothermal and adiabatic bed with gas and solid conduction; there is no heat exchange between the gas phase and the environment; constant diffusivity model; lumped resistance model with linear driving force; equilibrium relations for both components are represented by the Extended Langmuir-Freundlich model; column pressure drop is expressed by Ergun equation.

The column was configured to be initially saturated with 50 % methane and 50 % carbon dioxide. The inlet specifications of the single and multi component system as the valves organization of the simulation are summarized in Appendix F.

4.1 Breakthrough simulation

In the first place, a breakthrough test was made for the single component adsorption, using toluene as a reference component. A breakthrough curve is a plot of the concentration of the adsorbate in the effluent stream, which is, in this case, methane, carbon dioxide, and toluene, as a function of time. To perform these simulations, the mass transfer coefficients needed to be estimated, as no compatible information was found in the literature. Therefore, a first estimation of the MTC values was obtained following the equations presented in Appendix G.

It should be noted that the breakthrough time is determined by equilibrium and kinetic parameters. In terms of the equilibrium factor, the isotherm curve is the parameter that impacts the variance of the stoichiometric time. Regarding the kinetics factors, the axial dispersion, the mass transfer resistance in the film and inside the particles, and the heat transfer dictate the breakthrough time.

As the feed flow, the diameter, and the height of the column are relatively high, the components' removal on the modelled TSA will mainly be based on the equilibrium separation. That means that the kinetic factors will not significantly influence the VOCs and siloxanes removal.

When the MTC assumes a relatively low value, a dispersive wave can be created in the column. This occurs because greater concentrations travel at a slower rate than lower concentrations.

An abrupt front is created when the MTC present a high value, and the dispersion coefficient a relatively lower one. Due to the sharp front, numerical problems might arise, leading to simulation problems of some breakthroughs. This did happen with the k_{LDF} estimated parameter, not being able to run the simulation until rupture of toluene. The simulation did crash just in the moment before its rupture from the bed, and to prevent this, the MTC value was reduced. This approach was followed from estimated to the highest MTC value that would allow the toluene to exit the column. It is worth noting that the ratio between these two values was used to calculate methane and carbon dioxide MTC values. The respective breakthrough curve is presented in Figure 4.1 a), where the considered values of MTC for methane, carbon dioxide, and toluene were $3.3 \times 10^{-3}\,\mathrm{s}^{-1}$, $1.4 \times 10^{-3}\,\mathrm{s}^{-1}$, and $9.8 \times 10^{-5}\,\mathrm{s}^{-1}$, respectively. To understand if the assumed MTC of toluene would create some dispersive phenomena inside the column, three distinct values were considered on node 16, for comparison purposes, and is presented in Figure 4.1 b).

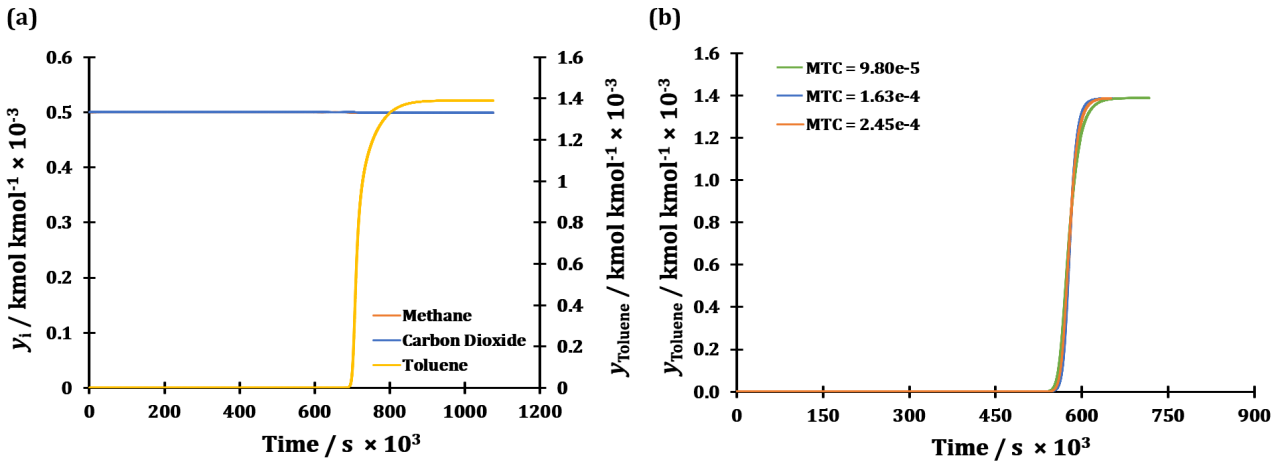

Figure 4.1: Breakthrough curve for toluene (a) in the end of the column and (b) in node 16.

One can see from the right-hand figure, that no substantial differences appear between the MTC values, showing that there is no significant dispersing phenomenon, the 2.45×10^{-4} was the estimated value and is represented by the orange line. It is also reasonable to conclude from this experiment that MTC values can assume different values, up to a given limit, without substantial present discrepancies. With this in mind, the assumed values for the MTC of toluene are valid for the single component adsorption simulations.

4.2 Single component adsorption

Removal of toluene was studied in the first place, in order to validate the implemented model with field data. The same operating conditions were assumed for the model as the same dimensions of the column from the benchmark used for a biogas plant. Some differences rely on the adsorbent material that is used. Both materials are activated carbon based, presenting similar dimensions and specific surface areas. However, nothing can be said related to the composition, meaning that different

chemical groups will be present in the carbons. This will indeed influence the adsorption and desorption efficiency of the adsorbate. The major purpose is to determine whether similar results of the same order of magnitude were obtained.

A biogas inlet flowrate of $70\,\mathrm{kmol\,h^{-1}}$, which corresponds to approximately $1800\,\mathrm{Nm^3\,h^{-1}}$, was defined and is assumed as a fixed value. To regenerate the column, a purge flow gas composed by 3 % of methane and 97 % of carbon dioxide was considered. This stream is a by-product of the *Carborex MS* system that integrates the upgrading step of the biogas flow. The regeneration temperature that was considered, as similar as the one used to obtain the field data, was 493 K.

The model is configured as a three-column system, with each unit completing a three-step cycle in 24 hours. The steps are time-equalized, resulting in an eight hour duration for each. In the first place, a 27-cycle simulation was performed. As there are always two columns operating at the same time with the purge stream, it needed to be split in two, for the heating and the cooling steps of the columns.

A comparison of the last four cycles, in terms of temperature and column composition profile obtained at the end of the heating stage is presented in Figure 4.2.

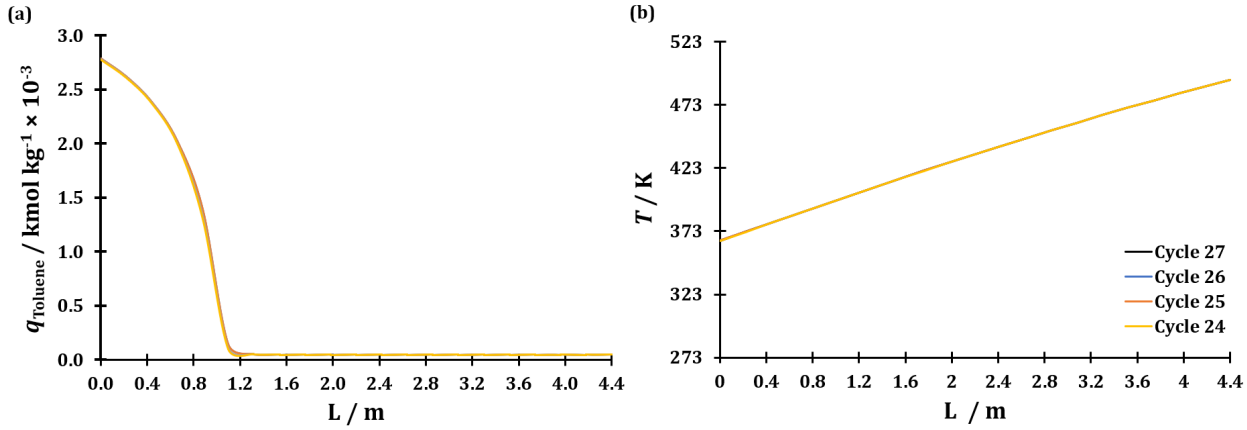

Figure 4.2: Last four cycle comparison of the (a) composition and (b) temperature column profile at the end of the heating step.

It is feasible to claim that no noticeable changes happened in both profiles, meaning that the TSA may have reached a Cyclic Steady-State (CSS). An important remark should be made to the temperature profile, where it is possible to check that the bottom temperature did not reach the regeneration temperature implied by the purge stream. The regeneration is indeed one of the challenges of a TSA, as uniform heating of the column is difficult to achieve. One of the consequences of the lack of heating at the bottom of the column is a drop in regeneration efficiency caused by the lowering in temperature.

Table 4.1 summarizes the data obtained for both TSA models in the waste stream, just before the cooling process began, with an attained steady state.

Table 4.1: The model and benchmark operating conditions.

	$\mathbf{Y_{Toluene}}$ $\mathbf{(kmol\,kmol^{-1})}$	**Temperature (K)**	**Presure (bar)**	**Flowrate** $\mathbf{(kmol\,h^{-1})}$
Model	66.54×10^{-4}	370	1.00	14.10
Benchmark	33.92×10^{-4}	413	1.14	28.85

One can conclude from these results that an amount of recovered toluene of the same order of magnitude was obtained, validating in a way the constructed TSA model.

A representation of the toluene molar fraction history in the waste stream is presented in Figure 4.3, for the last four simulated cycles.

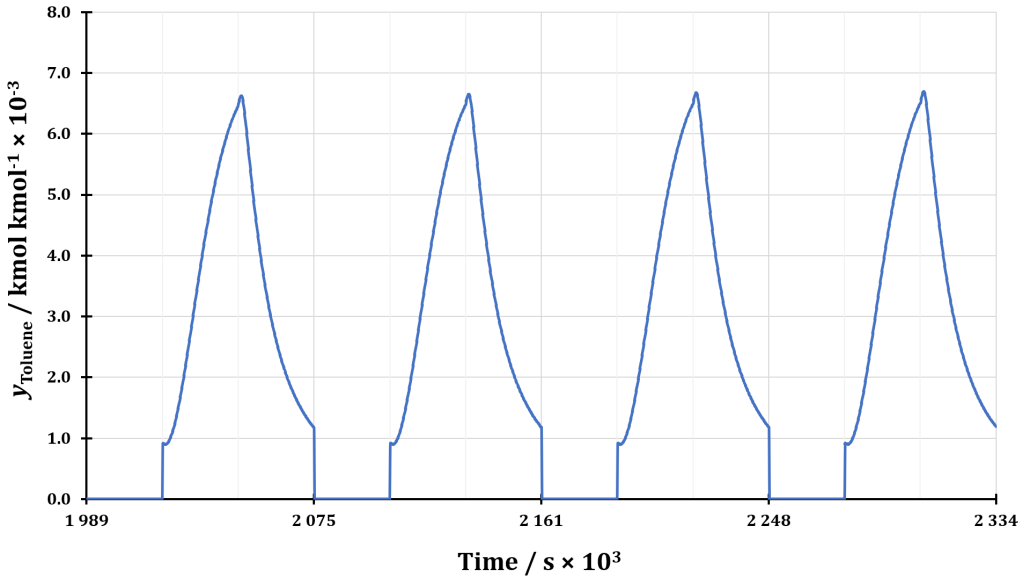

Figure 4.3: Last four cycle of the toluene composition in the waste stream.

Since the flow rate in the outlet stream is not constant, the computation of the released amount of toluene during the regeneration and cooling step could not be made directly from the molar fraction curve. As a result, the trapezoidal rule was used to calculate the integral area under the toluene flow rate curve for the four final cycles. The average amount of toluene removed in the regeneration and cooling stages was 0.769 kmol per cycle, corresponding to a total mass of 71.7 kg. The three-column system removed 215 kg of toluene every 24 hours, yielding a toluene desorption efficiency of 100 %.

We could infer from the collected results that the column could be oversized, as the toluene front did not achieve 30 % of the total length. However, single component adsorption can not be used to draw any definitive conclusions, as toluene can not accurately represent the totality of the VOCs. The other existing components in the inlet gas flow have different physical properties and varied affinities with the activated carbon. In this regard, multi-component adsorption must be done to draw further conclusions.

4.3 Multi component adsorption

Multi-component adsorption simulations arise to understand how the adsorption and desorption phenomena vary with different components. Because of the different affinities of the molecules in the mixture, competitive adsorption occurs in binary and multi-component adsorption. When the concentration of VOC vapors with higher adsorption affinity reaches a particular threshold, competitive binding occurs, and molecules with lower adsorption affinity are replaced. The molecular weight, boiling point, and polarity degree of each compound can influence this adsorption capacity.

Simulations were made with the presence of three more VOCs and one siloxane as mentioned before. Since the inlet compositions will present some changes, all the compounds have to fulfill the total amount of VOCs that is represented by the toluene in the single component adsorption. As a consequence the concentration of each compound will be lower, which will have an influence on the MTC of each compound. As it was seen in section 4.1, changing the values of MTC will not present any significant dispersive phenomena. Therefore, an individual test for each compound with the respective concentration was made in order to understand which MTC value would allow a simulation run without any converging interruptions. The assumed MTC values for the methane, carbon dioxide, D-Limonene, 1-Butanol, D4 and toluene were $3.34 \times 10^{-4}\,s^{-1}$, $1.42 \times 10^{-4}\,s^{-1}$, $1.00 \times 10^{-4}\,s^{-1}$, $9.00 \times 10^{-5}\,s^{-1}$, $5.00 \times 10^{-5}\,s^{-1}$ and $5.00 \times 10^{-5}\,s^{-1}$, respectively.

As the complexity of the system changed by adding more components to the software, some changes in the solver settings were made, particularly in the tolerances. The settings window is presented in the Appendix H, which in turn presents the tolerances values used for the performed simulations.

4.3.1 Three column configuration scheme

For the first three-column configuration (C3.1), the same operating conditions as the cycles time-step shown in SC adsorption were maintained. Time-step scheduling was required to transform a single simulated TSA column into a three-column set-up, with all the units operating simultaneously. The scheduling was made for a twenty-four-hour cycle, depicted in Figure 4.4. The enumeration (I), (II), and (III) represent the adsorption, regeneration, and cooling steps, respectively. Each block represents an operation time of eight hours.

Bed 1	(I)	(II)	(III)
Bed 2	(III)	(I)	(II)
Bed 3	(II)	(III)	(II)

Figure 4.4: TSA time scheduling for the three column configuration.

Initially, a simulation of 39 cycles was conducted. The last four performed cycles were considered for comparison purposes to see whether the TSA had reached the cyclic steady-state. Figure 4.5 depicts the temperature and pressure history of the column during these last cycles. For a better

interpretation of the graphs, each mark on the x axis represents a complete cycle, and the smallest each constituent step.

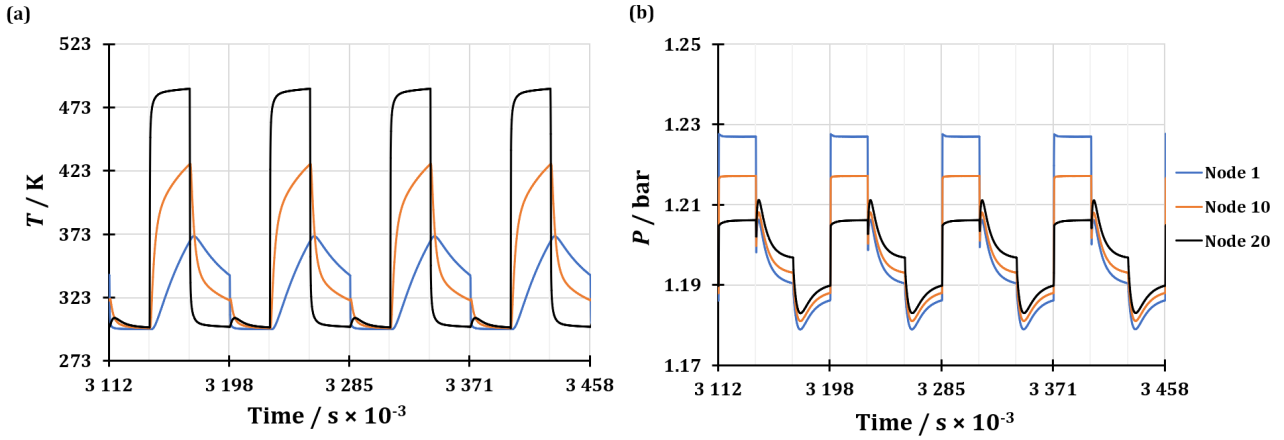

Figure 4.5: Last four cycle comparison of the (a) temperature and (b) pressure history of the column.

The left chart shows that a maximum temperature of 373 K was obtained at the bottom of the column. As this temperature is below the siloxane's and the terpene's boiling point, it is possible to draw early conclusions on the possible reduction on removal efficiency, specially in the beginning of the column.

The right chart, which represents the pressure for the defined nodes over time, shows a maximum pressure decrease of about 0.02 bar throughout the column during the adsorption step. Because the purge flow is significantly lower than the inlet flow, the velocity in the inlet will decrease, resulting in an overall decrease in pressure along the column, on the regeneration and cooling steps.

For a better understanding of the components' adsorption behaviour, an analysis of the solid loading throughout the column was done and represented in Figure 4.6.

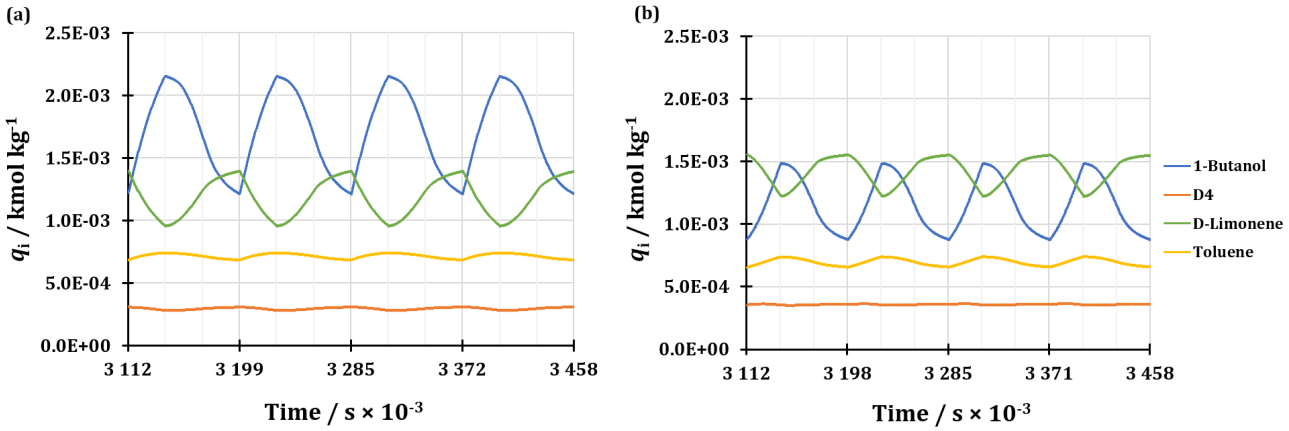

Figure 4.6: Components' loading comparison in the bed for the column's node (a) 1 and (b) 2, for configuration C3.1.

The first conclusion that can be rapidly retained from this graphs, is that D-Limonene and butanol are the two compounds that are most adsorbed in the beginning of the column. Looking with particular attention for Figure 4.6 a), one can see that the limonene's curve seems to be out phased from the other components' curves. In this node, when the adsorption step occurs, the butanol loading in the solid increases, resulting in a drop in limonene's adsorption. In the regeneration stage, however, this logic is reversed. This could lead to make some inferences, either this is related to a competitive adsorption phenomena or it is related to an error in the equilibrium or kinetic input data.

To understand why the terpene presented this behaviour in the bottom of the column, a deeper analysis on its adsorption history was done. Figure 4.7 presents the limonene's solid loading along the time, for different column nodes.

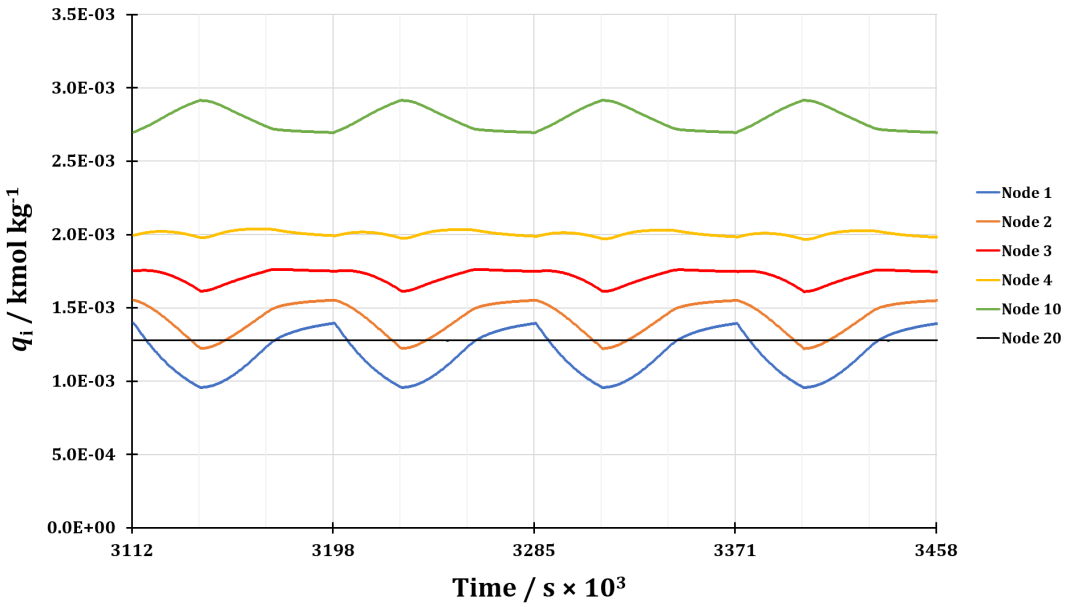

Figure 4.7: D-Limonene's solid loading history for the last four simulated cycles.

From this chart, it is noticeable that curves from the first to the forth column node follow the same behaviour, i.e., in the adsorption step a decrease in loading occurs and the opposite in the heating and cooling stage. It is important to remark, that these are the nodes where the butanol's loading peaks are higher. Looking now for the tenth node, a changing in the curves shape is noticed. In this case, in the adsorption step an increasing in the loading is experienced and the opposite for the remaining steps. This is indeed, the behaviour that the other components present in node one and two. In this sense, a competitive adsorption phenomena could be happening in the beginning of the column, mainly between the butanol and the terpene. This phenomenon begins to ameliorate when the butanol's adsorption decreases, starting from the forth node of the column.

Regarding the isotherms presented in Chapter 3, one can see that butanol and toluene are the compounds that show a higher maximum adsorption capacity. Therefore a higher affinity is followed by the butanol. Thus, competitive binding occurs when the concentration of butanol vapors reaches

a particular threshold, and terpene molecules with lower adsorption affinity are replaced, and move ahead in the carbon bed.

The competitive adsorption phenomenon and limonene's lower regeneration capacity depicted by the respective boiling point, lower vapor pressure and higher inlet concentration might enhance this compound capacity to move forward in the column. Therefore, the solid loading of the terpene in the next node, evidenced in Figure 4.6 b), presents a higher value than the other molecules. In this sense, for the subsequent nodes, it is predictable that most of the components will be rarely adsorbed in the carbon, except for the terpene.

Figure 4.8 displays the carbon loading (q_i) of each component at the end of the cooling stage, as a function of the column height, to provide a better perspective on the composition profile of the packed bed, on the last performed cycle.

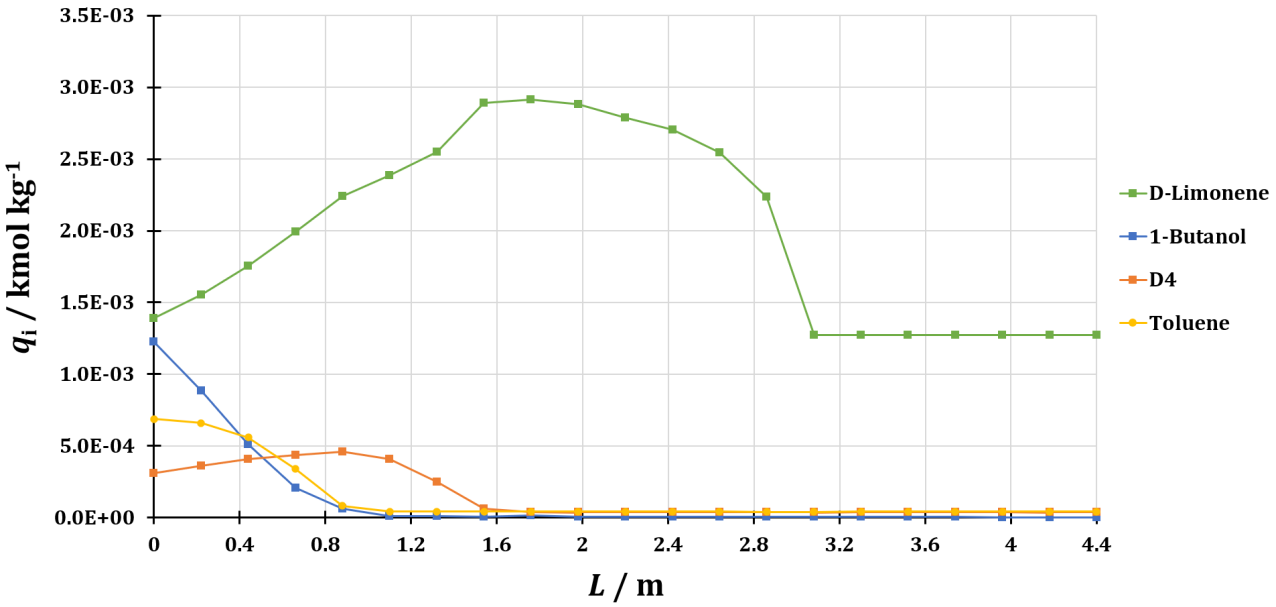

Figure 4.8: Composition profile of the column for C3.1 configuration scheme.

One can see from this figure, that the limonene front should be carefully controlled as the terpene appear to move faster than the other components, as stated before. The regeneration of this component group will be challenging since they present a high affinity with the packed bed and a higher boiling point, which hinders the desorption process. Hence, special consideration should be given to the terpenes, as they may exhibit a high adsorption rate and a lesser desorption/regeneration capacity.

Looking closely at the siloxane isotherm in Figure 3.1, one can see that this compound has a lower adsorption capacity. As a result, it is expected to advance faster in the column. In this case, the DMT client biogas contained a relatively low concentration of this compound, causing the front of this group to move slower than it would with a higher concentration. Therefore, it is important to do an evaluation of the concentration ranges that the TSA model can handle, specially for the siloxanes and the terpenes group, to still produce a good product quality.

This configuration allowed a safety factor of 32 %, which is determined by the ratio between the remaining column length that was not reached by the impurities and the total length.

An analysis of the waste stream of the column was made to verify the recovery capacity of the set configuration. As similar as the SC adsorption, a calculation of the amount of removed components is made when computing the integral area above the flow rate curves of each compound along the time. Figure I.1 from Appendix I represents the molar fraction of each compound with time. The presented data is useful to understand which compounds are removed in higher quantities. Clearly, the inlet concentration of each component influences this, since a higher input of a compound is evidenced by a higher integral area under the curve. Therefore, butanol presents a higher peak, followed by the D-Limonene, the toluene and then the siloxane.

Looking carefully to the components curve, one can observe that the respective peaks present the same value for the last cycles. This might be an indicator that after 39 days of operation, the column had already reached the cyclic steady-state.

In order to understand how efficient is the configuration C3.1, Table 4.2 shows the removed amount of each component in moles (n_i) and kg (m_i) in the heating and cooling step as the recovery percentage of the system, per column in each cycle.

Table 4.2: Performance results obtained for configuration C3.1.

Components	$\mathbf{n_{W1,i}}$ **(kmol)**	$\mathbf{m_{W1,i}}$ **(kg)**	$\mathbf{n_{F1,i}}$ **(kmol)**	**Recovery (%)**
Toluene	0.058	5.32	0.058	99.19
D4	0.030	8.78	0.032	91.49
D-Limonene	0.24	32.5	0.24	99.46
1-Butanol	0.48	35.6	0.48	100
Total	0.81	82.2	0.81	99.63

From the acquired results, the current design resulted in a total removal percentage of 99.63 % and the elimination of 82.2 kg of pollutants per column, resulting in a total of 247 kg per day.

On the combination of the heating and cooling steps, the component D4 showed the lowest recovery efficiency, which can be explained by their higher boiling point and molecular weight. Compounds with a higher boiling point are more challenging to regenerate because it is more difficult to volatilize and desorb from the stable state created with the adsorbent. Species with a higher molecular weight are more difficult to regenerate as they strain to be removed from the micropores. The remaining compounds present a similar removal percentage and are near the complete regeneration.

From the recovery percentages it is possible to see that the siloxane present a weaker capacity to desorb in the performed conditions. As this compound keep accumulating each cycle, a change in the regeneration step has to be considered. A more efficient regeneration step should be planned, as the lowered removed compounds inlet concentration variations can cause significant issues in the light product, resulting in membrane clogging with time. Adjusting the temperature or the flow rate of the purge stream or the duration of the heating stage can be considerable changes to optimize this phase,

being maybe the easiest parameters to adjust. Changing the type of the purge stream can also be an option, for example, by steam, which in turn can present a higher heat transfer capacity. Other decision making, such as increasing the height of the column, can be designed to enhance the safety factor. This fact, however, may increase resistance to heat transfer to the bottom of the column.

As increasing the regeneration time will present some obstacles on the time scheduling of the three columns, this option can be discarded for now. Nonetheless, a simulation test should be performed to determine whether decreasing the cooling stage significantly impacts the components' concentration front progress, as a lower adsorption capacity is expected.

Increasing the regeneration flow rate might be ideal, as only a modification in the valve system is needed. The problem attained to this option is that it will depend on the stream that comes from the membrane stage. Some studies related to this recycling should be done, to understand the ranges that the purge stream can operate.

A time-step rearrangement was made for an alternative three column configuration (C3.2) to understand the component behaviour with a different schedule. In this new configuration, two columns are adsorbing simultaneously with half of the flow rate while the other column will regenerate and cool down with the total purge flow rate. A TSA scheduling of the alternative configuration is presented in Figure 4.9 for a better understanding, where each block represents a duration of two hours.

Bed 1	(I)	(I)	(I)	(I)	(I)	(I)	(I)	(I)	(II)	(II)	(II)	(III)
Bed 2	(II)	(II)	(II)	(III)	(I)	(I)	(I)	(I)	(I)	(I)	(I)	(I)
Bed 3	(I)	(I)	(I)	(I)	(II)	(II)	(II)	(III)	(I)	(I)	(I)	(I)

Figure 4.9: TSA time scheduling for configuration C3.2.

The main difference of this configuration relays on the regeneration step, as it will have a lower duration, as the same as the cooling step. Regarding the cooling stage, a decrease in column cooling efficiency is expected, which could affect the next cycle's adsorption step. The adsorption step presents a lower inlet flow, however its duration was doubled. For the second case, the same operating conditions were applied as the first configuration, excepting the inlet flow and the time steps duration.

A simulation of 28 cycles was performed, and the final four cycles of the history and pressure history were presented as similar as the first configuration, and it is shown in Figure 4.10.

When comparing these plots with the charts of configuration C3.1, certain discrepancies can be depicted. The temperature history, as predicted, displays considerable changes, particularly on the cooling stage, as the first node of the column only reached a temperature of 376 K at the end of the cycle. Also, in the endings of the heating stage, a temperature of around 387 K was achieved, lading to an increase of 17 K while comparing to the first configuration. As just half of the inlet is considered in this situation, a lower pressure drop throughout the column is presented as a overall decrease in pressure range.

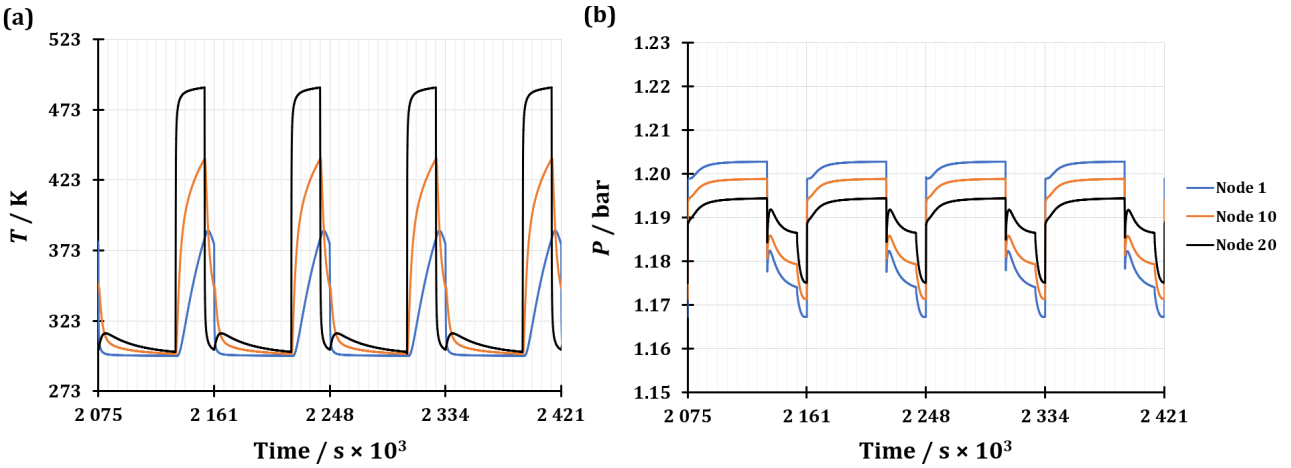

Figure 4.10: Column's (a) temperature and (b) pressure history for configuration C3.2.

An analysis of the solid loading throughout the column in the last four cycles is represented in Figure 4.11. It depicts the adsorption capacity of each component in different column nodes for this configuration, and the configuration presented in the first place (C3.1).

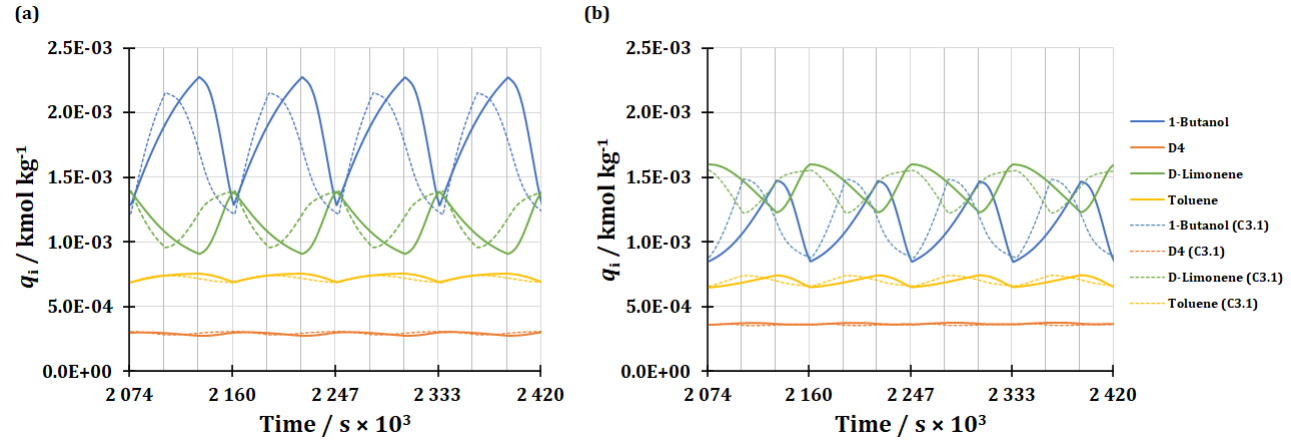

Figure 4.11: Components loading comparison in the bed for the column's node (a) 1 and (b) 2, for the present configuration and C3.1.

There is no noticeable changes on the adsorption on the first two nodes of the column. The competitive adsorption phenomena is still present mainly between the terpene and the butanol. However, an overall analysis of the column's composition profile should be done to understand the advance of the concentration front.

Figure 4.12 shows the composition profile of the column at the end of the last cycle.

Comparing both profiles, it is possible to state that a lower advanced front is evidenced for configuration C3.2. However, it is still not known if the CSS was achieved as in configuration C3.1, therefore, no further conclusions can be made in this sense. The same conclusions may be drawn from this graph as the ones taken from the composition profile of the first configuration. The presence of limonene

in the bed is evident, since it accounts for over 68 % of the length of the column, complying with a safety factor of around 36 %. Once again, the D-Limonene is the compound that will cause a greater concern while designing this set-up.

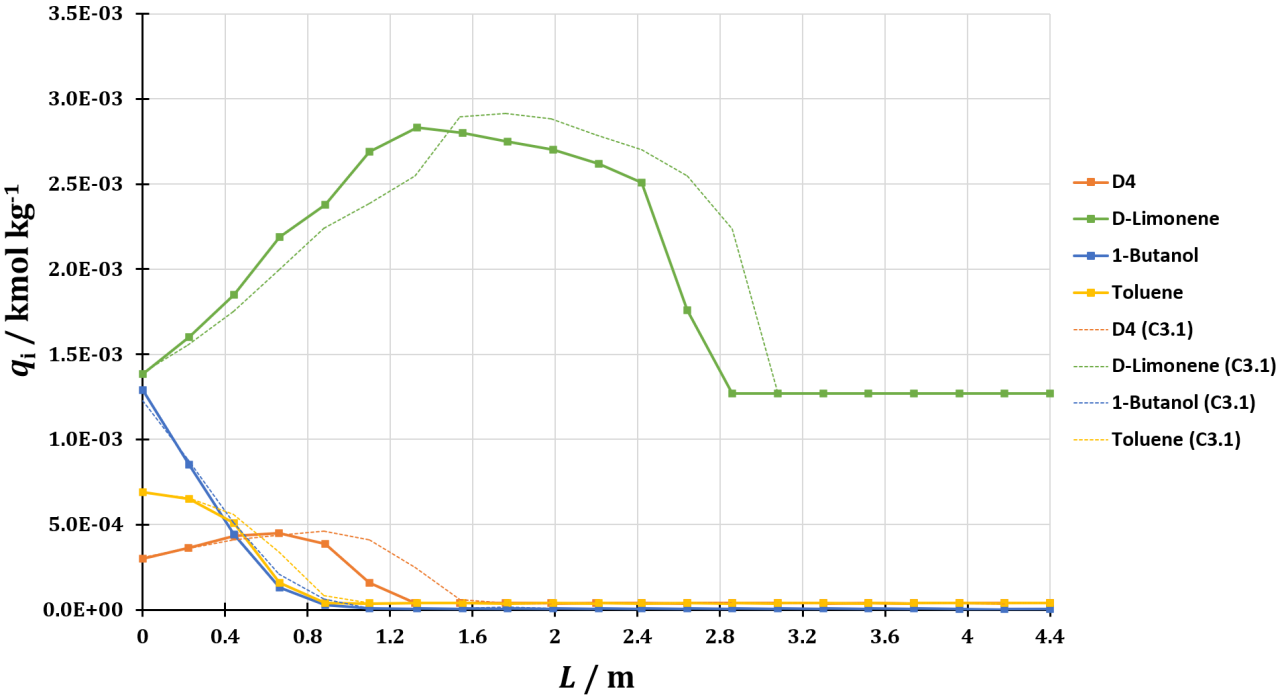

Figure 4.12: Composition profile of the column for the present configuration and C3.1.

Figure I.2 from Appendix I represents the molar fraction of each compound in the waste stream throughout the time. Limonene's curve peaks again revealed that, unlike the other species, this compound did not achieve a steady state. A longer simulation should be performed to understand when the terpene would have reached the steady state. Having an overall look, the maximum molar fraction for the four components was lower in this configuration than the first one, which can be explained by the lower volume of packed bed that was reached by the adsorbed components. Looking carefully for the compounds curves, the peaks for butanol, siloxane and toluene did not achieve their maximum value, as their curve does not start to decline before the cooling step changes. Therefore, for C3.2 set-up, extending the time cycle duration with the same operating conditions can actually be a better solution which will allow an increase of the area under the curve, and therefore, hindering the accumulation of certain components.

The regeneration capacity of the system can be estimated by some calculations following the same reasoning as the first configuration. Table 4.3 displays the recovered amount of each component in the heating and cooling step as the recovery percentage, per column in each cycle.

Table 4.3: Performance results obtained for configuration C3.2.

Components	$\mathbf{n_{W1,i}}$ **(kmol)**	$\mathbf{m_{W1,i}}$ **(kg)**	$\mathbf{n_{F1,i}}$ **(kmol)**	**Recovery (%)**
Toluene	0.051	4.70	0.058	87.63
D4	0.021	6.31	0.032	65.72
D-Limonene	0.18	25.1	0.24	76.75
1-Butanol	0.43	31.8	0.48	89.61
Total	0.69	67.9	0.81	84.70

As in the preceding arrangement, butanol and toluene have a larger recovery percentage, whereas siloxane and terpene trail in this regard. This design combined a total recovery percentage of 85 % and a total mass removal of 67.9 kg of pollutants, for a total of approximately 204 kg for the three columns scheme. This poor results mainly result from the lowering time operation of the heating stage. A higher maximum of pollutants molar fraction in the waste stream was experienced which means that this configuration could work with the same operating conditions but with a longer regeneration time. This could prevent or slow the rapid advance of components front inside the column.

This design presents a stronger adsorption capacity of the adsorbate in the first nodes of the column, however, the steady state was not reached, suggesting that greater buildup is expected from all of the components, particularly the siloxane and terpene. Therefore, no solid conclusions can be taken in terms of the safety factor that this design might accomplish at that time, rather than stating that it will be lower than 36 %. Certain issues are connected to the variation in concentrations, namely of limonene and siloxane, as an increase in their inlet concentrations might cause a disruption on the CSS and thus an advance of the components throughout the column. This will make this configuration even less safer than C3.1. To avoid this potential problems some changes on the regeneration should be considered as either increasing the flow rate, the temperature of the heating step.

As an overall revision, it is possible to infer that the regeneration step conditions area pivotal for an efficient TSA model. The accumulation of limonene could be depicted mainly in the plot of the molar fraction of the waste stream on configuration C3.2. This was also evidenced by the removal percentages that were calculated for this component that were around 80 %. In addition to this compound, the siloxane also showed some poor removal results, which also indicates that this component kept accumulating inside the column. As it is present in lower concentrations, this phenomena was hardly spotted, however analysing these components solid loading in a forward node is helpful to drawn some conclusions. Figure 4.13 depicts the loading of the siloxane with time in node four and five for configuration C3.1 and C3.2, respectively.

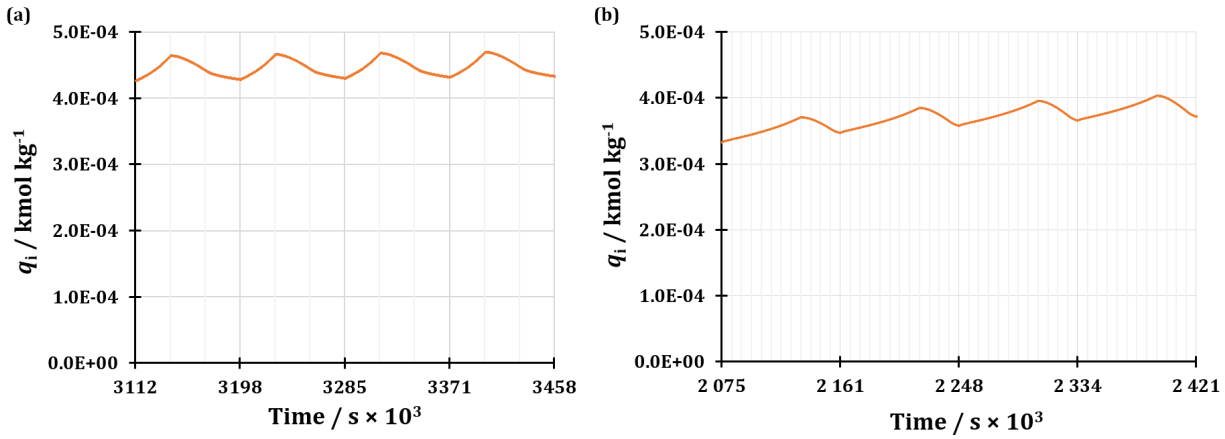

Figure 4.13: Last four cycle of D4's loading history in (a) node 5 for configuration C3.1 and (b) node 5 for configuration C3.2.

As expected, a continuous accumulation of the siloxane is noticed along the time and it is more noticeable in configuration C3.2. Once again, the accumulation of this compound is explained by the poorer regeneration efficiency, which in turn is intimately related to the higher boiling and molecular mass. Some consideration should also be given to this component's group, since a change in the inlet composition, originating from a different feed stock, might result in a poor light product quality, as soon as this compound starts to leave the column.

4.3.2 Two column configuration scheme

The two column layout is regarded as an alternative design for the biogas processing stage. The two column design was also used as a comparative approach, with two distinct time step configurations. A cycle of 24 hours was also considered, as in the previous subsection.

To transform a single simulated column into a two-column configuration (C2.1), a time-step scheduling was done and it is illustrated in Figure 4.14. For this TSA scheduling, two columns operate continuously and each block represents a duration of six hours.

Bed 1	(I)	(I)	(II)	(III)
Bed 2	(II)	(III)	(I)	(I)

Figure 4.14: TSA time scheduling for the two-column configuration C2.1.

In this set-up, the adsorption stage takes up half of the total cycle time, while cooling and heating are time-equalized at six hours. A simulation of 31 cycles was performed, and the final four cycles of the history and pressure history are displayed in Figure 4.15.

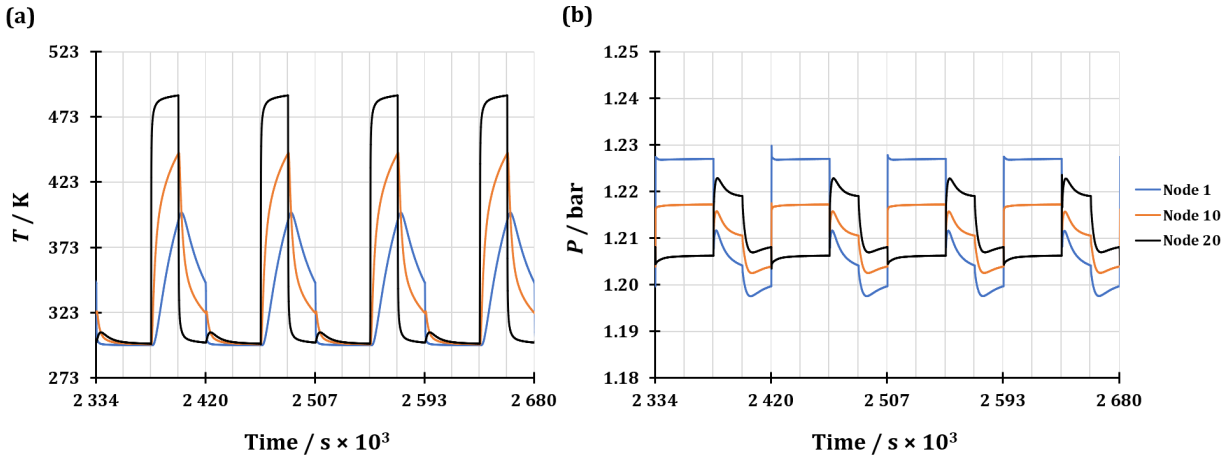

Figure 4.15: Column's (a) temperature and (b) pressure history for the two-column configuration C2.1.

The temperature history shows that towards the end of the regeneration process, the first node of the column reached a maximum temperature of 400 K. It is a significant variation from the purge temperature, which will impact the components' removal, as it was seen in the three column configurations. Relatively to the pressure history chart, identically to the configuration (C3.1), a maximum pressure drop of roughly 0.02 bar was experienced along the column.

The adsorption capacity history is represented in Figure 4.16 for the first and second node.

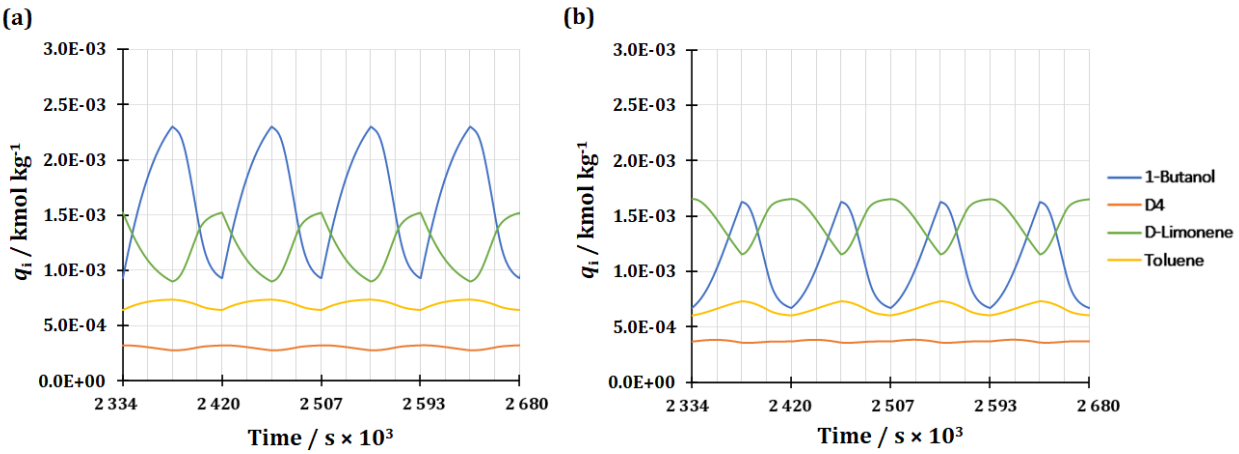

Figure 4.16: Components' loading in the bed for node (a) 1 and (b) 2 of configuration C2.1.

Noting this figure, one can see that once again, D-Limonene and butanol were the two components with a higher solid loading, as they also present a higher inlet concentration. It is also depicted in this design the competitive adsorption phenomena. At this time, toluene starts to mark some importance in this matter besides butanol, as a higher adsorption capacity is evidenced. Compared to Figure 4.11, the components curves exhibit similar behavior and values for the first two nodes concerning the configuration C3.2. This could be explained by the regeneration step, as it presents the same

operating conditions. However, it does not mean that the composition profile of the column will be similar for both configurations. In configuration C2.1, the adsorption step is made with twice the inlet flow rate, which is expected to cause a higher advance in the components concentration front.

Figure 4.17 represents the axial composition profile of the column at the end of the cooling step, for the last simulated cycles.

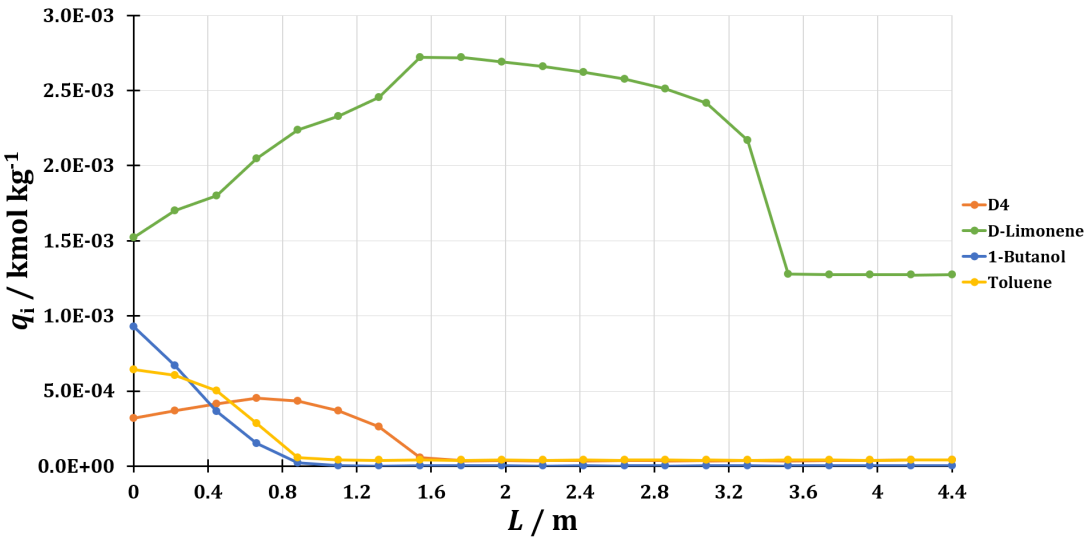

Figure 4.17: Composition profile of the column for the present configuration and C2.1.

One can see that the components front present a higher advance in this configuration compared to the previous presented ones. This verifies what was said before, as a higher adsorption time will cause a higher adsorption in the carbon bed. This time, the terpenes front reached 80 % of the total length of the column which makes up for 20 % of safety factor for this design. Other components like the siloxane presented also a considerable advance in this set-up.

Figure I.3 from Appendix I represents the molar fraction of each compound in the waste stream along the time. Noting this figure, no evident signs exist to claim that the steady state was not achieved, unlike the other configurations. However, deeper analysis needs to be done to draw any further conclusions. For this case, a higher amount of components is expected to be removed per column, as a higher duration of the adsorption step was set, injecting more flow inside the column. Therefore a higher integral area is expected under the component's curve. For this configuration, the molar fraction curve of each component presents a descendant behaviour before the beginning of the cooling step, with an exception of the toluene. This means that the majority had achieved the maximum removal, however, due the cooling step, a sharp decrease on the molar fraction was experienced. For the improvement of the heating step, either the elongation of the heating step could be considered, therefore smoothing the descending slope, or increasing the regeneration temperature. More inferences related to this stage can be made after the analysis of the recovery percentages.

The regeneration performance of the system was estimated, following the same reasoning as the other configurations. Table 4.4 shows the recovered amount of each component in moles (n_i) and kg

(m_i) in the heating and cooling step as the removal percentage for the same steps, per column in each cycle.

Table 4.4: Performance results obtained for configuration C2.1.

Components	$\mathbf{n_{W1,i}}$ **(kmol)**	$\mathbf{m_{W1,i}}$ **(kg)**	$\mathbf{n_{F1,i}}$ **(kmol)**	**Recovery (%)**
Toluene	0.074	6.82	0.087	82.47
D4	0.035	10.4	0.049	70.44
D-Limonene	0.28	38.1	0.36	79.00
1-Butanol	0.60	44.5	0.72	84.22
Total	0.92	99.8	1.2	82.00

This configuration presents the overall poorest removal efficiency from the presented set-ups, where the siloxane presents a lower removal percentage. Clearly some changes need to be done for the improvement of this setup. As configuration C3.2, the heating stage was inefficient since the temperature in the entrance was either near or below the boiling point of the components. Only six hours were considered for the regeneration, however if a longer time was considered, a higher amount of compounds could be removed, as explained before. Another way to solve the lower removal efficiency is to enhance the purge temperature or flow. As the limonene front reached a relatively high value of the column length, an elongation of the column could also be considered, avoiding the rupture of the impurities and contamination of the light product. This alternative, however, will cause a higher pressure drop (increasing operating costs with the blower) and a poorer heat transfer. For this design, an overall removal efficiency of 82 % was obtained giving a total of 100 kg of removed compounds per column and a total of 200 kg per cycle.

From configuration C2.1, one can see that the main problem relayed on the heating step, and therefore some changes need to be made in this matter. For the improvement of the TSA performance, a time-step optimization was performed for another configuration and the respective TSA scheduling is presented in Figure 4.18. Each block represents a duration of three hours.

Bed 1	(I)	(I)	(I)	(I)	(II)	(II)	(II)	(III)
Bed 2	(II)	(II)	(II)	(III)	(I)	(I)	(I)	(I)

Figure 4.18: TSA time scheduling for configuration C2.2.

For configuration C2.2 an enhancement of the regeneration step duration was made to study the influence on the removal performance. Therefore, in the present configuration, an heating step of nine hours was considered, decreasing therefore the cooling time for three hours, as the adsorption step remained constant.

A simulation of 28 cycles was performed, and the final four cycles of the history and pressure history are displayed in Figure 4.19.

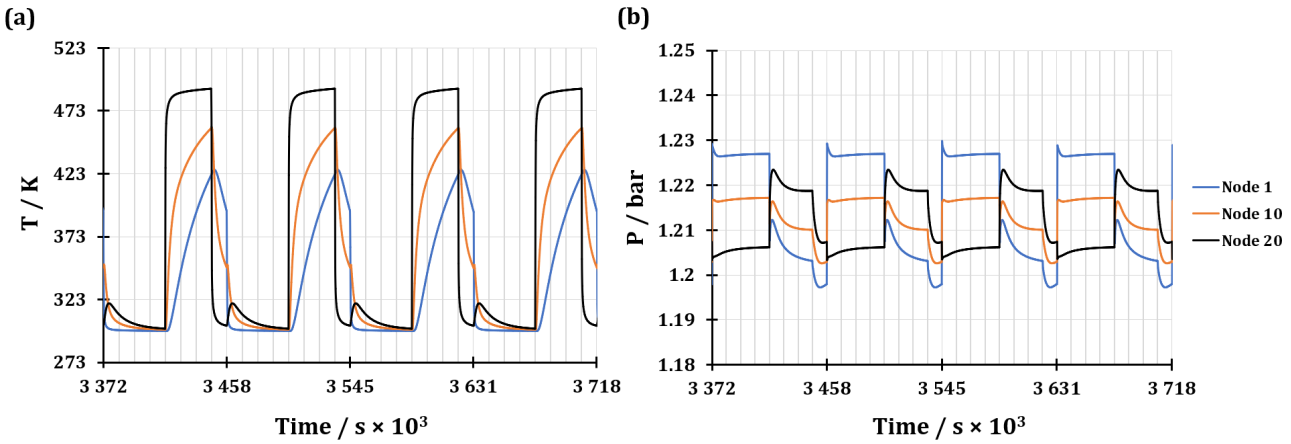

Figure 4.19: Column's (a) temperature and (b) pressure history for configuration C2.2.

This time-step design achieved a maximum temperature of 423 K in the intake, with a gap of 50 K to the purge stream, making this the most efficient configuration on the heat transfer inside the column. However, the inlet did not undergo a proper cooling down at the end of the cooling step, reaching a temperature of 393 K. As soon as the adsorption starts, the hot gas will move up with a higher temperature, which justifies the bump in the last node curve at the beginning of the next cycle. Regarding the right chart, a pressure drop of 0.02 bar was experienced through the column as similar as configuration C2.1 and C3.1.

A representation of the solid loading throughout the column in the last four cycles for configuration C2.2 and C2.1 is represented in Figure 4.20.

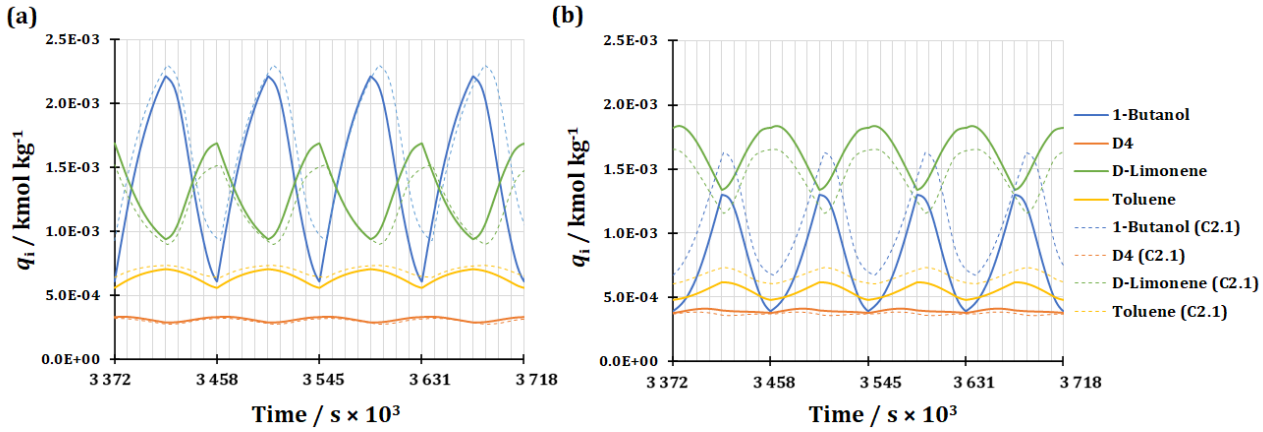

Figure 4.20: Components' loading in the bed for the column's node (a) 1 and (b) 2, for configuration C2.2 and C2.1.

Once again, all of the components behave in the same way as those in the other arrangements. Overall, no significant differences between the two column arrangements can be seen, meaning that reducing the cooling time had no significant effect in the components' adsorption for the first nodes.

However this is not enough to draw any final conclusions. In this sense, an overall analysis needs to be done to the composition profile of the column.

Figure 4.21 depicts the axial composition of the column as a function of its length and the composition profile obtained for the previous configuration.

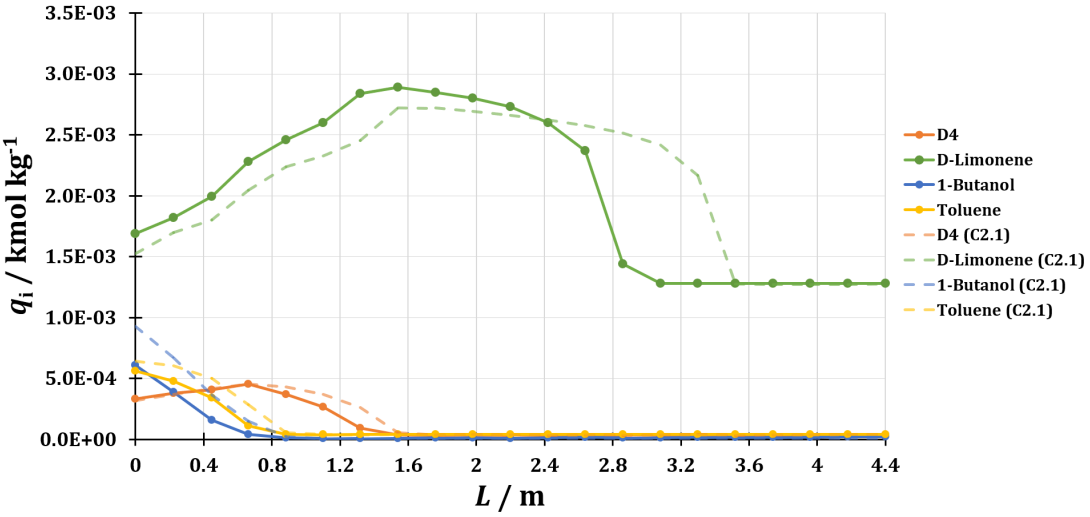

Figure 4.21: Composition profile of the column for the present configuration and C2.1

One can see that a safety factor of roughly 32 % was obtained for the configuration C2.2. A significant difference is noticed between the two column designs. With this data, one can conclude that the regeneration stage will determine the column composition profile, as a lag in the composition front of the constituents is observed. Raising the regeneration duration step by 3 hours, which corresponds to a 50 % increase in time, enhanced the safety factor by about 18 %. Despite the fact that there was an improvement on the column safety factor, the light product stream temperature increased by at least 20 K. Temperature variations will affect the membrane selectivity integrated in the next up upgrading stage, demanding further cooling of this outflow stream.

Figure I.4 from Appendix I represents the molar fraction of each compound in the waste stream along the time. No clear signs exist to claim that the steady state was not achieved from this graph, like the previous configuration. For the current set-up, a higher amount of components is expected to be recovered per column, since a lag of the concentration front was observed due to the increment of the regeneration time.

The regeneration performance of the system was estimated, following the same reasoning as the other configurations. Table 4.5 displays the removed amount of each component in moles (n_i) and kg (m_i) in the heating and cooling step as the recovery percentage for the same steps, per column in each cycle.

Table 4.5: Performance results obtained for configuration C2.2.

Components	$\mathbf{n_{W1,i}}$ **(kmol)**	$\mathbf{m_{W1,i}}$ **(kg)**	$\mathbf{n_{F1,i}}$ **(kmol)**	**Recovery (%)**
Toluene	0.086	7.89	0.087	98.05
D4	0.046	13.5	0.049	93.84
D-Limonene	0.35	47.8	0.36	97.57
1-Butanol	0.71	52.4	0.72	98.41
Total	1.19	122	1.21	97.95

From the acquired results, the current design resulted in a total recovery percentage of 98 % and the elimination of 122 kg of pollutants per column, resulting in 244 kg per cycle. Increasing the duration of the regeneration step showed a significant influence on the recovery of the components, achieving almost the percentage of total removal of the impurities from the packed bed. The component that once again showed a lower removal percentage, even though in a lower range for this configuration, was the siloxane. A slight increase in the regeneration time could lead to more efficient removal of this component, as the temperature at the beginning of the column would be near the siloxane's boiling point.

While comparing configurations with two and three columns, some pros and cons can be depicted.

Regarding the three-column configuration, the C3.1 set-up was the one that showed a higher removal efficiency. This study showed that this set-up performance could be improved if either the regeneration time or the purge temperature or flow-rate were slightly higher. Also, good safety factor percentages were obtained for this design, being suitable for biogas flows or plants that tend to have significant fluctuations on the feed stock. However, the major disadvantage of the three-column set-up relies on the capital and operating costs, as an additional column needs to be built and the maintenance costs increase. Therefore, an optimization could be done to the benchmark configuration, which would, however, impact the operating costs.

Relatively to the two-column scheme, the C2.2 set-up showed the best removal performance, being also the configuration with the highest regeneration step. It is the ideal configuration as it presents lower investment costs and higher removal efficiency. However, configuration C2.1 present lower safety factors which will imply lower safety margins, if some considerable changes occur in the inlet stream concentrations. Also, some changes should be made in the structure of the column, as either a larger diameter or height should be considered for a higher carbon volume availability. Carbon loses efficiency with time, increasing the danger of a component rupture if the inflow concentration is changed. For a more efficient recovery, a regeneration step with a higher time, temperature (below the carbon's ignition temperature), and purge flow should be done between a couple of cycles. Configuration C2.1, however, should be considered for smaller plants with lower biogas flows and lower inlet concentration fluctuations, for safety reasons.

For the purge flow, it was considered a by-product of the upgrading unit, having the advantage of re-utilizing this stream instead of it being released directly into the air. However, as shown from

the presented results, this flow did not show an efficient heat transfer. Thus, it will either imply the implementation of a higher heating and cooling stage duration or an increase in the purge flow. Other different purge streams are used in some systems, such as nitrogen or steam, which will indeed imply extra costs. However, they present a more efficient heat transfer along the column that will allow a reduction of the purge flow. Air could be another gas mixtures that could be tested in the TSA unit, presenting an advantage related to the acquisition costs. However, while using air, some concerns should be considered as hot spots can be created, namely the ketones when exposed to air residues, which could cause an ignition of the carbon bed. In this case, temperature control should be associated with the system along the column to avoid the packed bed to ignite.

4.4 Parametric study

A parametric study emerges as a method to improve the TSA performance in removing the impurities from the biogas flow and studying the influence of these parameters in the same unit. Having this in mind, different parameters were considered to be studied as the inlet velocity (u_0), the regeneration temperature (T_{reg}), the ratio between the purge and inlet flow (P_{u}/F) and the length of the column (L).

This study was made for configurations C3.1 and C2.2, which were the best performed configurations from the three and two column scheme, respectively.

Changing the inlet velocity of the system implies changing the packed bed volume available for the adsorption. If the velocity is lower, then the diameter is higher, as the inlet flow is fixed, and therefore there is an increase in the available packed bed volume.

Higher temperatures will be favorable as the endothermic regeneration stage will be more efficient, resulting in a greater amount of pollutants being collected in the waste stream. However, this can not be extended indefinitely since energy consumption grows exponentially and higher temperature can ignite or damage the adsorbent. Having a close look to the components properties in Appendix B, one can see that the highest boiling point corresponds to the siloxane's with 448.55 K. This gives an idea of the minimal regeneration temperature that should be used in this step.

Varying the P_{u}/F ratio will also impact the regeneration step and the cooling step in addition. As the inlet flow (F) is a fixed value, only the purge flow (P_{u}) will vary in this case. It is expected that with a higher purge flow, the regeneration and cooling steps become more efficient, as the counter current flow achieves faster the bottom of the column.

The column length is always adjusted to fit the current system. The effects of increasing and decreasing this parameter will be different. If the height is increased, the column will have a larger packed bed volume and the safety factor will raise. However, the higher pressure drop along the column implies a higher investment and operational cost. It also hinders heat transfer within the column during the heating and cooling stages. On the other hand, if the column length is reduced, the safety factor becomes this approach main disadvantage. Allowing, however a more efficient heat transfer and lowers the investment costs.

4.4.1 Three column configuration (C3.1)

The standard velocity employed was 0.150 m s^{-1}, and simulations with a decrease of 15 % (Run 1) as well as increases of 15 % (Run 2) and 30 % (Run 3) were performed. For the standard velocity, around 4.5 m^3 of carbon is available inside the column. For the remaining simulated velocities a total quantity of 5.3 m^3, 3.9 m^3 and 3.4 m^3 of carbon was disposed for Run 1, Run 2 and Run 3, respectively.

In order to study the influence of the temperature decrease in the systems' regeneration, a temperature of 480 K (Run 4), 465 K (Run 5) and 450 K (Run 6) on the purge flow were considered for these simulations.

A standard purge flow of 28.2 $kmol\,h^{-1}$ was considered, and an increase of 20 % (Run 7), and a decrease of 25 % (Run 8), and 50 % (Run 9) relatively to the standard value were studied. This corresponds to a purge flow (P_u) of 34 $kmol\,h^{-1}$, 21 $kmol\,h^{-1}$ and 14 $kmol\,h^{-1}$ for Run 7, Run 8 and Run 9, respectively.

The standard length of the column was 4.40 m, and a decrease of 10 % (Run 10), 20 % (Run 11) and 25 % (Run 12) was performed, giving a total height of 3.96 m, 3.52 m and 3.30 m, respectively. A total volume of 3.96 m^3, 3.52 m^3 and 3.30 m^3 of packed bed is available for Run 10, Run 11 and Run 12, respectively.

The obtained results of the parametric study for the three-column configuration are summarized in table 4.6. A simulation of 31 cycles was performed for each presented run.

Table 4.6: Results obtained for the parametric study of configuration C3.1.

Run	u_0 ($m\,s^{-1}$)	T_{reg} (K)	P_u/F	L (m)	Recovery (%)	Safety Factor (%)
Standard	**0.15**	**493**	**0.40**	**4.40**	**95**	**55**
1	**0.13**	493	0.40	4.40	96	55
2	**0.17**	493	0.40	4.40	95	49
3	**0.20**	493	0.40	4.40	93	30
4	0.15	**480**	0.40	4.40	90	51
5	0.15	**465**	0.40	4.40	84	43
6	0.15	**450**	0.40	4.40	73	34
7	0.15	493	**0.48**	4.40	97	**58**
8	0.15	493	**0.30**	4.40	94	40
9	0.15	493	**0.20**	4.40	93	32
10	0.15	493	0.40	**3.96**	97	44
11	0.15	493	0.40	**3.52**	98	46
12	0.15	493	0.40	**3.30**	**99**	39

From the presented results, the best recovery percentage was achieved by using a smaller column, where it is implicit that a better heat transfer was achieved. In fact a temperature of around 440 K was achieved in the bottom of the column justifying the higher removal efficiency by this set-up.

A higher safety factor was achieved for the configuration with a higher purge flow. This result also makes sense as a higher flow in counter current, will allow a faster column heating, specially in the bottom which is the most difficult part. For this configuration, a temperature of 430 K was obtained in the end of the heating cycle. One can see that increasing the purge flow rate between some operating cycles could avoid an early replacement of the bed, increasing the carbon life time, and therefore, decreasing the respective acquisition costs. Nonetheless, this can not be increased indefinitely, as the purge stream in this system is a by-product of the upgrading unit. Other regeneration type of streams can be used, and should be studied like steam or air, that are not depending on the system.

In a general way, the inlet velocity variation influenced more the safety factor comparing to the recovery percentage, as a lower volume of bed is disposed and no changes were made in the heating and cooling steps. The temperature, as expected showed a big importance on the TSA recovery performance. Decreasing the regeneration temperature by 9 % resulted in a 23 % removal efficiency loss. It is imperative to choose the correct operating temperature, and, therefore, more studies relatively to the increase of temperature should be done.

To optimize this configuration, a combination of a slight increase in purge flow and regeneration temperature, as well as a decrease in column length, should be tested. In addition, the regeneration step timing can be studied, as increasing the cycle time for more than 24 hours may have a positive effect on the optimization step.

4.4.2 Two column configuration (C2.2)

As for the two-column configuration different results were obtained, as a lower safety factor, other variations were made to the parameters under study. Simulations with a decrease of 15 % (Run 13) as well as increases of 15 % (Run 14) and 25 % (Run 15) were performed. For the standard velocity around 4.5 m^3 of carbon is available inside the column and for the remaining simulated velocities Run 13, Run 14 and Run 15 a total quantity of 5.3 m^3, 3.9 m^3 and 3.6 m^3, respectively, of disposed carbon.

In order to study the influence of the temperature decrease in the systems' regeneration, a temperature of 480 K (Run 16), 465 K (Run 17) and 450 K (Run 18) on the purge flow were considered for these simulations.

As the standard purge flow was 28.2 $kmol\,h^{-1}$, an increase of 20 % (Run 19), and a decrease of 25 % (Run 20), and 50 % (Run 21) relatively to the standard value was studied. This corresponds to a purge flow of 34 $kmol\,h^{-1}$, 21 $kmol\,h^{-1}$ and 14 $kmol\,h^{-1}$ for Run 19, Run 20 and Run 21, respectively.

The standard length was of the column was 4.40 m, and a decrease of 10 % (Run 22), 20 % (Run 23) and 25 % (Run 24) was performed, giving a total height of 3.96 m, 3.74 m and 3.52 m, respectively. A total volume of 3.96 m^3, 3.81 m^3 and 3.58 m^3 of packed bed is available for Run 22, Run 23 and Run 24, respectively.

The obtained results of the parametric study for the three-column configuration are summarized in table 4.7. A simulation of 31 cycles was performed for each presented run.

Table 4.7: Results obtained for the parametric study of configuration C2.2.

Run	u_0 ($m\,s^{-1}$)	T_{reg} (K)	P_u/F	L (m)	Recovery (%)	Safety Factor (%)
Standard	**0.15**	**493**	**0.40**	**4.40**	**98**	**32**
13	**0.13**	493	0.40	4.40	**99**	36
14	**0.17**	493	0.40	4.40	97	25
15	**0.19**	493	0.40	4.40	94	14
16	0.15	**480**	0.40	4.40	91	30
17	0.15	**465**	0.40	4.40	88	27
18	0.15	**450**	0.40	4.40	77	20
19	0.15	493	**0.50**	4.40	**99**	**39**
20	0.15	493	**0.30**	4.40	97	25
21	0.15	493	**0.20**	4.40	96	8
22	0.15	493	0.40	**3.96**	98	30
23	0.15	493	0.40	**3.74**	**99**	30
24	0.15	493	0.40	**3.52**	**99**	23

The same conclusions can be drawn for the two-column configuration as the ones taken from configuration C3.1. As expected, more runs achieved a higher recovery efficiency in this set-up while varying different parameters. Decreasing the inlet velocity and the column height as increasing the purge flow were as similar to the previous presented parametric study, the variations that would enhance the TSA performance.

From the presented data, one can see, that decreasing the bed height for 3.52 m, does not give extra advantages to the system as a safety factor of 23 % is achieved. Therefore, the best height from the three performed ones would be with 3.74 m presenting a higher recovery percentage and a relatively lower safety factor compared to the standard configuration.

An important remark should be done to Run 19, where the highest recovery and safety factor percentage was achieved. The purge flow shows a big influence on the TSA performance, specially in the safety factor value, as reducing the flow rate by 25 % and 50 % will cause a lowering of 22 % and 75 %, respectively, in the safety factor. For Run 21, probably before the moment that the CSS would have been achieved, the rupture of the terpene or other compounds would be experienced for this configuration.

It would be highly recommended, specially for the two-column system to perform a purge step with higher duration and flow-rate in between some operating cycles. This will make the bed more efficient along the time, avoiding an early replacement of the carbon. Also, it will avoid a bed quality product on the light stream, and therefore prevent the membranes clogging in the upgrading system. In short, this procedure could avoid extra operating costs related to maintenance and replacement of the packed bed and the membranes stages.

Chapter 5

Conclusions

Aspen Adsorption V12 was used to simulate a TSA technology for removing VOCs and siloxanes in the pre-treatment stage of a biogas process. The BG flow available for the treatment process was 70 kmol h^{-1}, which equates to around 1800 Nm^3 h^{-1}. The simulations accounted for a total concentration of 1388 ppm of VOCs and roughly 6 ppm of siloxanes.

Due to the high simulation run time, only three volatile organic compounds were considered. The compounds 1-Butanol, toluene, and D-Limonene were added to the model representing the oxygenated, aromatics, and terpene group, respectively. Octamethylcyclotetrasiloxane, also known as D4, was introduced to the system to represent the siloxanes.

Single component adsorption was performed in the first place, following the same operating conditions as a benchmark, where toluene was considered to represent the totality of 1388 ppm of VOCs. The primary purpose of this simulation was to validate the model using the benchmark's reference TSA system. A three-column configuration was adopted, similar to the benchmark, with the same time-step scheduling. Each stage lasted 8 hours, using a regeneration temperature of 493 K. From this simulation, results of the same order of magnitude were obtained, validating the built TSA model.

As a SC adsorption was not representative of all the impurities behavior and affinity with the packed bed, an MC adsorption was performed.

A three-column configuration was tested in the first place, similar to the benchmark setup. The configuration C3.1 achieved a total recovery percentage of 100%, a removed amount of 247 kg for the three columns per cycle, and a safety factor of 32%. Butanol, toluene and the terpene almost reached complete regeneration. However,the siloxane was the compound that showed a lower recovery efficiency, intimately associated with their higher boiling point (consequent lower vapor pressure) and molecular weight. These results implied that some changes should be made in the regeneration step. Therefore, increasing the regeneration temperature, flow-rate or the heating time duration could be two possible and quick changes to the system that would enhance the TSA performance. A higher regeneration temperature would require higher hot utilities, leading to higher operational costs. Increasing the heating time would impact the cooling step, lowering the safety factor. However, as it was proven afterwards with configuration C2.2 results, the heating step presents a higher weight in enhancing the safety factor. Increasing the flow rate may be the simplest adjustment to implement

in the system, while increasing the regeneration time would pose some issues with the TSA time-scheduling. A second three-column design was also tested, where the inlet flow was divided into two columns while the third was regenerating and cooling down. With a total amount of 204 kg of removed compounds and a reduced safety factor of 36%, this configuration achieved recovery effectiveness of 85%. The difference in the safety factor and removal performance between the two setups can be explained by the fact that in set-up C3.2 did not reahched the CSS, so it is expected a lowering of the safety factor value.

When compared with the three-column scheme, a two-column design was tested to understand the adsorption and desorption differences. Configuration C2.1 was firstly performed, where it was considered adsorption of 12h and regeneration and cooling time of 6 hours each. Similar to configuration C3.2, a total recovery percentage of 82% was achieved, conceiving an amount of 200 kg of removed impurities, implying a safety factor of 20%. To improve the TSA performance, a time-step optimization was done in configuration C2.2. As the problem relayed on the regeneration step, an elongation of the duration of this stage was considered. This was also an interesting study to understand if the decrease of the cooling time would present any impact on the advance of the components concentration front. For the C2.2 setup, a total removed percentage of 98% was achieved, combined with a total amount of 244 kg of impurities removed, complying with a safety factor of 32%. This difference is justified by an increase in the heating step-time, demonstrating that a longer regeneration time has a more significant impact than reducing the cooling on the components progress inside the column, complying with a 60% improvement in the safety factor. Despite the fact that there was an improvement on this parameter, an increase of the light product stream temperature was experienced, demanding further cooling of this outflow stream due to membrane selectivity reduction.

In short, configurations C3.1 and C2.2 should be used for higher biogas flows as a higher safety is associated with it. However, the fist configuration presents a drawback related to the investment cost associated with an extra column. An occasional purge with higher duration, temperature, and flow should be done between cycles to prevent an early replacement of the packed bed material.

With the parametric study performed on configurations C3.1 and C2.2, it was possible to conclude that: increasing the inlet biogas flow velocity and decreasing the purge flow provoke a more significant influence on the safety factor rather than the recovery efficiency; reducing the regeneration temperature showed a massive impact on the recovery percentage of the system; decreasing the column length allowed achievement of a higher recovery efficiency due to the improvement on the heat transfer. However, a lowering of the safety factor is associated.

The purge stream under study provided good performance, particularly in configurations C3.1 and C2.2, where CSS was almost attained, also complying with a good safety factor. One downside of using the by-product stream of the membranes stage as a purge flow is that its flow-rate can not be infinitely increased. Another purge stream, such as steam, should be examined for comparison reasons, as it may demonstrate higher heat transfer, allowing for an earlier CSS attainment and lower acquisition costs.

Chapter 6

Assessment of the work done

6.1 Objectives achieved

The main objectives achieved on this work relied on: the familiarization with the *Aspen Adsorption* software; finding in the literature for carbon based adsorbents with available adsorption equilibrium data for most of the compounds present in the biogas stream of the DMT client; modelling of a three step TSA model for a three and two column configuration; carrying out a parametric study to understand the influence of different parameters in the TSA performance.

6.2 Limitations and future work

Modelling a TSA requires a lot of experimental data related to the adsorbent, and equilibrium and kinetic data of the compounds in study. Therefore, finding this information in the literature appears as a limitation of this work, as the information was also not found from the same article or author. Hence, the data used are from different sources which will affect the final data.

Beyond this, no isotherm was found for the siloxane D4 in the BPL carbon, as the made assumption did not have any valid foundation beyond. Also, regarding the D-Limonene component, the respective equilibrium data was only available for a temperature of 298K, hence the model fitting in the experiment data was not as accurate.

Some changes to the system were required for the simulations to converge, resulting in a lower model accuracy.

As a future work, other purge streams should be evaluated for this system such as steam or air, as they might present a higher efficiency on the heat transfer, therefore reducing the necessity of a higher flow and regeneration temperature. More components should be added to the system for a better accuracy of the model. A non-adiabatic TSA column should also be tested to understand the influence of the heat loss along the walls on the regeneration step. Finally, an economical evaluation should be made for the three and two column configurations, facilitating afterwards the decision making when a biogas flow treatment with certain characteristics is required.

6.3 Final assessment

The work done provided an insight into the current challenges of VOCs and siloxanes removal from biogas. The lack of information related to the kinetic and equilibrium data appear as the biggest limitation of this work. Therefore, an experimental work, or data from an activated carbon supplier coupled to this project can bring more accuracy to the project. This work can be seen as a solid contribution for the development of a more efficient TSA model for the trace components removal.

References

[1] I. E. Agency, "Outlook for biogas and biomethane: Prospects for organic growth." University of Newcastle Upon Tyne. Available at https://www.iea.org/reports/outlook-for-biogas-and-biomethane-prospects-for-organic-growth/annex, 2020.

[2] S. Rasi, A. Veijanen, and J. Rintala, "Trace compounds of biogas from different biogas production plants," *Energy*, vol. 32, no. 8, pp. 1375–1380, 2007.

[3] U. Zavyalova, B. Nigrovski, K. Pollok, F. Langenhorst, B. Müller, P. Scholz, and B. Ondruschka, "Gel-combustion synthesis of nanocrystalline spinel catalysts for vocs elimination," *Applied Catalysis B: Environmental*, vol. 83, no. 3, pp. 221–228, 2008.

[4] L. Zhu, D. Shen, and K. H. Luo, "A critical review on vocs adsorption by different porous materials: Species, mechanisms and modification methods," *Journal of Hazardous Materials*, vol. 389, p. 122102, 2020.

[5] Y.-S. Son, K.-J. Kim, and J.-C. Kim, "A review on vocs control technology using electron beam," *Asian Journal of Atmospheric Environment*, vol. 4, pp. 63–71, 09 2010.

[6] M. GarcIa and D. Rico, "Presence of siloxanes in the biogas of a wastewater treatment plant separation in condensates and influence of the dose of iron chloride on its elimination," *International Journal of Waste Resources*, vol. 06, 01 2016.

[7] M. Ajhar, M. Travesset, S. Yüce, and T. Melin, "Siloxane removal from landfill and digester gas – a technology overview," *Bioresource Technology*, vol. 101, no. 9, pp. 2913–2923, 2010.

[8] C. S. R. Sá, "Developing a technological concept for the removal of siloxanes and vocs from landfill gas," Master's thesis, Faculdade de Engenharia da Universidade do Porto, Porto, 2021.

[9] F. A. Silva, "Developing a technological concept for the removal of vocs and siloxanes from landfill gas: solvent recovery," Master's thesis, Faculdade de Engenharia da Universidade do Porto, Porto, 2022.

[10] Y. Y. Kevin R. Wood, Y. A Liu, *Simulation of Adsorption Processes*, ch. 1, pp. 1–153. John Wiley Sons, Ltd, 2018.

[11] A. M. M. Mendes, *Laboratórios de Engenharia Química - Reatores em fase homogénea, reatores catalíticos, separações não convencionais e tecnologia dos sólidos particulados*. U.Porto Editorial, Second ed., 2019.

[12] A. Ghoshal and S. Manjare, "Selection of appropriate adsorption technique for recovery of vocs: an analysis," *Journal of Loss Prevention in the Process Industries*, vol. 15, no. 6, pp. 413–421, 2002.

[13] A. Science, "Outlook for biogas and biomethane: Prospects for organic growth." . Available at https://www.airscience.ca/blank-1?msclkid=e1c02c23bbf411eca25727e76636ab28, 2016.

[14] D. Ko, I. Moon, and D.-k. Choi, "Analysis of the contact time in a cyclic thermal swing adsorption process," *Industrial & Engineering Chemistry Research*, vol. 41, no. 6, pp. 1603–1615, 2002.

[15] "Choosing an adsorption system for voc: Carbon, zeolite, or polymers.," Technical Bulletin 456/F-99-004, Environmental Protection Agency, Durham, North Carolina, May 1999.

[16] X. Li, L. Zhang, Z. Yang, P. Wang, Y. Yan, and J. Ran, "Adsorption materials for volatile organic compounds (vocs) and the key factors for vocs adsorption process: A review," *Separation and Purification Technology*, vol. 235, p. 116213, 2020.

[17] Lenntech, "Adsorption / active carbon." . Available at https://www.lenntech.com/library/adsorption/adsorption.htm.

[18] X. Zhang, B. Gao, A. E. Creamer, C. Cao, and Y. Li, "Adsorption of vocs onto engineered carbon materials: A review," *Journal of Hazardous Materials*, vol. 338, pp. 102–123, 2017.

[19] Z. Zhu, H. Xu, J. Jiang, H. Wu, and P. Wu, "Hydrophobic nanosized all-silica beta zeolite: Efficient synthesis and adsorption application," *ACS Applied Materials & Interfaces*, vol. 9, no. 32, pp. 27273–27283, 2017. PMID: 28727415.

[20] H. Nigar, N. Navascués, O. de la Iglesia, R. Mallada, and J. Santamaría, "Removal of vocs at trace concentration levels from humid air by microwave swing adsorption, kinetics and proper sorbent selection," *Separation and Purification Technology*, vol. 151, pp. 193–200, 2015.

[21] D.-G. Lee, J.-H. Kim, and C.-H. Lee, "Adsorption and thermal regeneration of acetone and toluene vapors in dealuminated y-zeolite bed," *Separation and Purification Technology*, vol. 77, no. 3, pp. 312–324, 2011.

[22] P. Liu, C. Long, Q. Li, H. Qian, A. Li, and Q. Zhang, "Adsorption of trichloroethylene and benzene vapors onto hypercrosslinked polymeric resin," *Journal of Hazardous Materials*, vol. 166, no. 1, pp. 46–51, 2009.

[23] C. Long, Y. Li, W. Yu, and A. Li, "Removal of benzene and methyl ethyl ketone vapor: Comparison of hypercrosslinked polymeric adsorbent with activated carbon," *Journal of Hazardous Materials*, vol. 203-204, pp. 251–256, 2012.

[24] W.-Q. Wang, J. Wang, J.-G. Chen, X.-S. Fan, Z.-T. Liu, Z.-W. Liu, J. Jiang, and Z. Hao, "Synthesis of novel hyper-cross-linked polymers as adsorbent for removing organic pollutants from humid streams," *Chemical Engineering Journal*, vol. 281, pp. 34–41, 2015.

[25] S. Wang, L. Zhang, C. Long, and A. Li, "Enhanced adsorption and desorption of vocs vapor on novel micro-mesoporous polymeric adsorbents," *Journal of Colloid and Interface Science*, vol. 428, pp. 185–190, 2014.

[26] K. Vellingiri, P. Kumar, A. Deep, and K.-H. Kim, "Metal-organic frameworks for the adsorption of gaseous toluene under ambient temperature and pressure," *Chemical Engineering Journal*, vol. 307, pp. 1116–1126, 2017.

[27] M. Zhu, P. Hu, Z. Tong, Z. Zhao, and Z. Zhao, "Enhanced hydrophobic mil(cr) metal-organic framework with high capacity and selectivity for benzene vocs capture from high humid air," *Chemical Engineering Journal*, vol. 313, pp. 1122–1131, 2017.

[28] M. Shafiei, M. S. Alivand, A. Rashidi, A. Samimi, and D. Mohebbi-Kalhori, "Synthesis and adsorption performance of a modified micro-mesoporous mil-101(cr) for vocs removal at ambient conditions," *Chemical Engineering Journal*, vol. 341, pp. 164–174, 2018.

[29] E. Gabruś and D. Downarowicz, "Anhydrous ethanol recovery from wet air in tsa systems – equilibrium and column studies," *Chemical Engineering Journal*, vol. 288, pp. 321–331, 2016.

[30] G. Swetha, T. Gopi, S. Chandra Shekar, C. Ramakrishna, B. Saini, and P. Rao, "Combination of adsorption followed by ozone oxidation with pressure swing adsorption technology for the removal of vocs from contaminated air streams," *Chemical Engineering Research and Design*, vol. 117, pp. 725–732, 2017.

[31] N. Qi and M. D. LeVan, "Coadsorption of organic compounds and water vapor on bpl activated carbon. 5. methyl ethyl ketone, methyl isobutyl ketone, toluene, and modeling," *Industrial & Engineering Chemistry Research*, vol. 44, no. 10, pp. 3733–3741, 2005.

[32] S. M. Taqvi, W. S. Appel, and M. D. LeVan, "Coadsorption of organic compounds and water vapor on bpl activated carbon. 4. methanol, ethanol, propanol, butanol, and modeling," *Industrial & Engineering Chemistry Research*, vol. 38, no. 1, pp. 240–250, 1999.

[33] E. N. Rudisill, J. J. Hacskaylo, and M. D. LeVan, "Coadsorption of hydrocarbons and water on bpl activated carbon," *Industrial & Engineering Chemistry Research*, vol. 31, no. 4, pp. 1122–1130, 1992.

[34] S. Himeno, T. Komatsu, and S. Fujita, "High-pressure adsorption equilibria of methane and carbon dioxide on several activated carbons," *Journal of Chemical & Engineering Data*, vol. 50, no. 2, pp. 369–376, 2005.

[35] T. M. Tovar, *Adsorption Equilibria and Mass Transfer in Porous Adsorbents*. PhD thesis, Faculty of the Graduate School of Vanderbilt University, Nashville„ 2016.

[36] Y. He, J.-H. Yun, and N. Seaton, "Adsorption equilibrium of binary methane/ethane mixtures in bpl activated carbon: Isotherms and calorimetric heats of adsorption," *Langmuir : the ACS journal of surfaces and colloids*, vol. 20, pp. 6668–78, 09 2004.

[37] M. M. Davis and M. D. LeVan, "Experiments on optimization of thermal swing adsorption," *Industrial & Engineering Chemistry Research*, vol. 28, pp. 778–785, 1989.

[38] J. A. Delgado, V. I. Águeda, M. A. Uguina, J. L. Sotelo, P. Brea, and C. A. Grande, "Adsorption and diffusion of h2, co, ch4, and co2 in bpl activated carbon and 13x zeolite: Evaluation of performance in pressure swing adsorption hydrogen purification by simulation," *Industrial & Engineering Chemistry Research*, vol. 53, pp. 15414–15426, 2014.

[39] B. Boulinguiez and P. Le Cloirec, "Biogas pre-upgrading by adsorption of trace compounds onto granular activated carbons and an activated carbon fiber-cloth," *Water science and technology : a journal of the International Association on Water Pollution Research*, vol. 59, pp. 935–44, 02 2009.

[40] E. Glueckauf, "Theory of chromatography. part 10.formulæ for diffusion into spheres and their application to chromatography," *Transactions of The Faraday Society*, vol. 51, pp. 1540–1551, 1955.

[41] C. Sereno and A. Rodrigues, "Can steady-state momentum equations be used in modelling pressurization of adsorption beds?," *Gas Separation Purification*, vol. 7, no. 3, pp. 167–174, 1993.

[42] S. Azizian and S. Eris, "Chapter 6 - adsorption isotherms and kinetics," in *Adsorption: Fundamental Processes and Applications* (M. Ghaedi, ed.), vol. 33 of *Interface Science and Technology*, pp. 445–509, Elsevier, 2021.

Appendix A

Adsorbent selection

The components of a DMT client's biogas flow are listed in Table A.1. The components are given in order of concentration, from the highest to the lowest. The carbons for which an equilibrium data was obtained in the literature are denoted by the number "1". The total concentration was calculated with the overall amount of VOCs represented by the equilibrium data.

Table A.1: VOCs and siloxanes present in a biogas plant from a DMT client.

Compound	**Concentration (ppm)**	**BPL**	**NORIT**	**PICA**	**Ingevity**
1–Butanol	73.628	1 [1]	1 [6]	–	1 [12]
D–Limonene	36.869	1 [2]	–	–	–
Cumene	11.526	–	–	–	–
2–Carene	8.457	–	–	–	–
Toluene	8.425	1 [3]	1 [7]	1 [11]	1 [12]
Camphene	8.214	–	–	–	–
gamma–Terpinene	5.511	–	–	–	–
(+)–4–Carene	5.110	–	–	–	–
Ethanol	3.939	1 [1]	1 [8]	1 [11]	1 [12]
2–Butanone	3.778	1 [3]	1 [9]	1 [11]	1 [12]
Ethyl Hexanoate	2.812	–	–	–	–
3–Carene	2.749	–	–	–	–
Carbonyl Sulphide	2.506	–	–	–	–
2–Pentanone	2.313	–	–	–	–
Acetone	2.302	1 [4]	–	1 [11]	1 [12]
alpha–Phellandrene	2.111	–	–	–	–
Eucalyptol	2.018	–	–	–	–
p–Xylene	1.975	–	–	–	–
Undecane	1.960	–	–	–	–
2–Butanol	1.753	1 [3]	–	–	–

Compound	Concentration (ppm)	BPL	NORIT	PICA	Ingevity
Tricyclene	1.748	–	–	–	–
Acetaldehyde	1.395	–	–	–	–
Carbon Disulphide	1.364	–	–	–	–
Isobutene	1.354	–	–	–	–
beta–Pinene	1.308	1 [2]	–	–	–
Ethyl Acetate	1.143	–	–	1 [11]	–
Cyclohexane	1.142	–	–	–	–
4–Methyl–2–Pentanone	1.129	1 [3]	–	–	–
1–Propyl Acetate	1.044	–	–	–	–
Decalin	0.946	–	–	–	–
1–Butanal	0.864	–	–	–	–
Dodecane	0.856	–	–	–	–
Butyl Cyclohexane	0.732	–	–	–	–
Ethyl Benzene	0.713	–	–	–	–
Octane	0.660	–	–	–	–
Camphor	0.647	–	–	–	–
o–Xylene	0.599	–	–	–	–
Isobutane	0.561	–	–	–	–
2–Methyl Butane	0.448	–	–	–	–
Tridecane	0.408	–	–	–	–
Heptane	0.355	–	–	–	–
o–Ethyl Toluene	0.304	–	–	–	–
Benzene	0.296	–	–	–	1 [12]
2–Methyl Furan	0.295	–	–	–	–
Ethyl Butanoate	0.260	–	–	–	–
Methyl Butanoate	0.246	–	–	–	–
Pentane	0.225	–	–	–	1 [12]
2,3,3–Trimethyl	0.192	–	–	–	–
Hexane	0.192	1 [4]	1 [9]	–	1 [12]
D4	5	–	–	–	–
Total	214.382	133.323	89.962	19.587	92.785
CO2	50 % v/v	1 [5]	–	–	1 [12]
CH4	50 % v/v	1 [5]	1 [10]	–	1 [12]

[1] S. M. Taqvi, W. S. Appel, and M. D. LeVan, "Coadsorption of organic compounds and water vapor on bpl activated carbon. 4. methanol, ethanol, propanol, butanol, and modeling," Industrial & Engineering Chemistry Research, vol. 38, no. 1, pp. 240–250, 1999.

[2] T. M. Tovar, Adsorption Equilibria and Mass Transfer in Porous Adsorbents. PhD thesis, Faculty of the Graduate School of Vanderbilt University, Nashville, 2016.

[3] N. Qi and M. D. LeVan, "Coadsorption of organic compounds and water vapor on bpl activated carbon. 5. methyl ethyl ketone, methyl isobutyl ketone, toluene, and modeling," Industrial & Engineering Chemistry Research, vol. 44, no. 10, pp. 3733–3741, 2005.

[4] E. N. Rudisill, J. J. Hacskaylo, and M. D. LeVan, "Coadsorption of hydrocarbons and water on bpl activated carbon," Industrial & Engineering Chemistry Research, vol. 31, no. 4, pp. 1122–1130, 1992.

[5] J. A. Delgado, V. I. Águeda, M. A. Uguina, J. L. Sotelo, P. Brea, and C. A. Grande, "Adsorption and diffusion of h2, co, ch4, and co2 in bpl activated carbon and 13x zeolite: Evaluation of performance in pressure swing adsorption hydrogen purification by simulation," Industrial & Engineering Chemistry Research, vol. 53, no. 40, pp. 15414–15426, 2014.

[6] J. Nastaj, K. Witkiewicz, and M. Chybowska, "Modeling of multicomponent and multitemperature adsorption equilibria of water vapor and organic compounds on activated carbons," Adsorption Science & Technology, vol. 34, no. 2-3, pp. 144–175, 2016.

[7] J. Nastaj, B. Ambrożek, K. Witkiewicz, and J. Rudnicka, "Adsorption isotherms of propan-2-ol, methylbenzene, and tetrachloromethane on selected activated carbons," Journal of Chemical & Engineering Data, vol. 61, no. 10, pp. 3559–3569, 2016.

[8] E. Gabruś and D. Downarowicz, "Anhydrous ethanol recovery from wet air in tsa systems – equilibrium and column studies," Chemical Engineering Journal, vol. 288, pp. 321–331, 2016.

[9] Hori H, Tanaka I, Akiyama T. [Adsorption characteristics of organic solvent vapors on the fixed bed of activated carbon]. Sangyo Igaku. 1983 Sep;25(5):356-66. Japanese. doi: 10.1539/joh1959.25.356. PMID: 6668723.

A. V. Shkolin, I. E. Men'shchikov, E. V. Khozina, V. Y. Yakovlev, V. N. Simonov, and A. A. Fomkin, "Deformation of microporous carbon adsorbent sorbonorit-4 during methane adsorption," Journal of Chemical & Engineering Data, vol. 0, no. 0, p. null, 0.

[11] F. Delage, P. Pré, and P. Le Cloirec, "Mass transfer and warming during adsorption of high concentrations of vocs on an activated carbon bed: Experimental and theoretical analysis," Environmental Science & Technology, vol. 34, no. 22, pp. 4816–4821, 2000.

[12] L. Jia, J. Shi, C. Long, F. Lian, and B. Xing, "Vocs adsorption on activated carbon with initial water vapor contents: Adsorption mechanism and modified characteristic curves," Science of The Total Environment, vol. 731, p. 139184, 2020.

Appendix B

VOCs and Siloxanes' properties

Table B.1 lists the most prevalent VOCs and siloxanes found in landfills. Analyzing their physical properties allows for a better understanding of the adsorbent adsorption effectiveness. The values were respected to the boiling point, and vapor pressure was obtained using *ASPEN HYSYS V12*. The boiling point was obtained for a pressure of 1 bar and the vapor pressure for a temperature of 25 °C.

Table B.1: VOCs and siloxanes' physical properties.

Compound	**Molecular Formula**	**Molecular Mass** ($\mathbf{g\,mol^{-1}}$)	**Boiling Point** (**K**)	**Vapor Pressure** (**kPa**)	**Polar surface area** ($Å^2$)
Toluene	C_7H_8	92.14	383.28	4.08	0
1-Butanol	$C_4H_{10}O$	74.12	390.55	1.32	20.2
D-Limonene	$C_{10}H_{16}$	136.23	442.65	0.40	0
D4	$C_8H_{24}O_4Si_4$	296.61	448.55	0.18	36.9

Appendix C

Isotherm model fitting experiment

The Langmuir isotherm and Langmuir-Freundlich isotherm equations for the pure component is expressed in Equations C.1 and C.2, respectively.

$$q_{\mathrm{i}} = q_{\mathrm{i,sat}} \frac{b_{0,\mathrm{i}} \mathrm{e}^{-\frac{\Delta \mathrm{H_i}}{RT}} p_{\mathrm{i}}}{1 + b_{0,\mathrm{i}} \mathrm{e}^{-\frac{\Delta \mathrm{H_i}}{RT}} p_{\mathrm{i}}} \tag{C.1}$$

$$q_{\mathrm{i}} = q_{\mathrm{i,sat}} \frac{\left(b_{0,\mathrm{i}} \mathrm{e}^{-\frac{\Delta \mathrm{H_i}}{RT}} p_{\mathrm{i}} \right)^{t}}{1 + \left(b_{0,\mathrm{i}} \mathrm{e}^{-\frac{\Delta \mathrm{H_i}}{RT}} p_{\mathrm{i}} \right)^{t}} \tag{C.2}$$

The fitting experiment between the experimental data from the literature and the model is calculated according to Equation C.3 which, in turn, indicates the minimum sum of squares (SS) for three different temperatures, excepting the terpenes.

$$\mathrm{SS}(\%) = \left((q_{\mathrm{exp},1} - q_{\mathrm{mod,i}})^2 \right) \tag{C.3}$$

Table C.1 and C.2 depict the Langmuir and Langmuir-Freundlich isotherm parameters, respectively, for each component and the respective minimum sum of squares (SS) error.

Table C.1: Parameters for the Langmuir model for each component.

Compounds	$\mathbf{q_{sat}}$ (**kmol kg^{-1}**) $\times$ **10^3**	$\mathbf{b_0}$ (**bar^{-1}**)	**-ΔH** (**J mol^{-1}**)	**SS** (**%**)
Methane	5.54	1.43×10^{-4}	16455	4.44×10^{-7}
Carbon Dioxide	11.0	6.48×10^{-6}	23972	1.45×10^{-2}
D-Limonene	3.07	8.20×10^{-2}	47000	5.88×10^{-7}
1-Butanol	5.38	7.05×10^{-7}	58601	7.82×10^{-6}
n-hexane	3.06	9.96×10^{-3}	35799	4.11×10^{-6}
Toluene	4.26	1.76×10^{-5}	53694	1.84×10^{-5}

Table C.2: Parameters for the Freundlich-Langmuir model for each component.

Compounds	$\mathbf{q_{sat}}$ ($\mathbf{kmol\,kg^{-1}}$) $\times$ $\mathbf{10^3}$	$\mathbf{b_0}$ ($\mathbf{bar^{-1}}$)	$\mathbf{-\Delta H}$ ($\mathbf{J\,mol^{-1}}$)	**t**	**SS** (%)
Methane	6.35	1.12×10^{-4}	16279	0.78	1.59×10^{-7}
Carbon Dioxide	11.0	7.04×10^{-6}	23972	0.72	2.58×10^{-6}
D-Limonene	6.24	5.17×10^{-5}	47000	0.08	2.58×10^{-8}
1-Butanol	5.38	9.98×10^{-7}	58601	0.50	3.71×10^{-7}
n-hexane	3.63	1.78×10^{-6}	56573	0.35	5.54×10^{-8}
Toluene	5.52	1.88×10^{-5}	50085	0.33	1.55×10^{-6}

Appendix D

Aspen adsorption flowsheet

The flowsheet that is evidenced in Figure D.1 was used for the TSA simulation. It is composed by one adsorbent layer bed (B1), two gas tank voids (TD1 and TD2), two product streams (P1 and W1), two feed streams (F1 and F2), four gas valves (VF1, VP1, VF2 and VW1) and one cycle organizer.

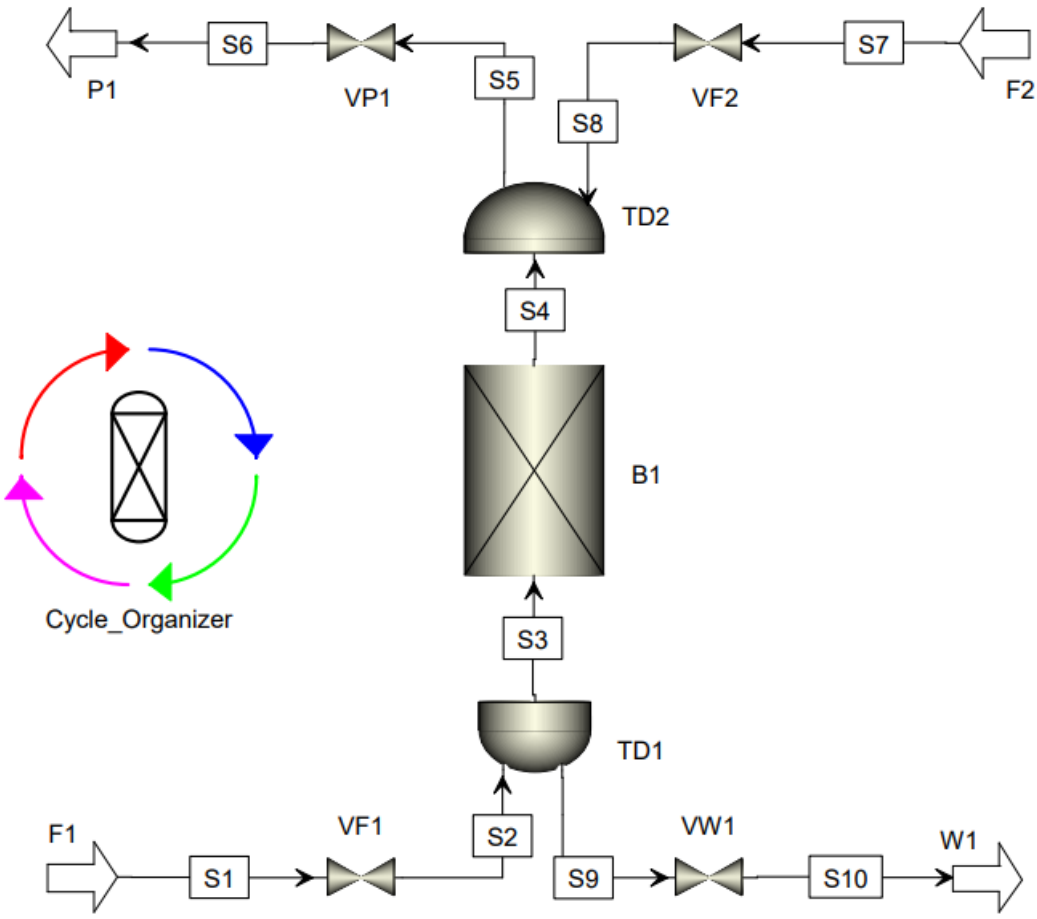

Figure D.1: Aspen Adsorption flowsheet.

Appendix E

Aspen Adsorption Input

E.1 Isotherm parameters

The following equations, E.1, E.2, E.3 and E.4 express the convertion of the isotherm parameters from Langmuir- Freundlich model to the extended Langmuir-Freudlich model used in Aspen Adsorption.

$$\mathrm{IP1} = q_{\mathrm{sat}} \tag{E.1}$$

$$\mathrm{IP2} = {b_0}^t = \mathrm{IP5} \tag{E.2}$$

$$\mathrm{IP3} = t \tag{E.3}$$

$$\mathrm{IP4} = \frac{-\Delta \mathrm{H} t}{R} = \mathrm{IP6} \tag{E.4}$$

E.2 Axial mass dispersion

The Einstein statistical theory of diffusion - random walk model was used to compute axial mass dispersion as it is expressed in Equation E.5

$$E_{\mathrm{z}} = \frac{u_{\mathrm{i}} d_{\mathrm{p}}}{2} \tag{E.5}$$

where u_{i} is the interstitial velocity and d_{p} is the adsorbent particle diameter.

E.3 Thermal conductivity

The gas and solid thermal conductivity can be expressed by equation E.6 and E.7.

$$Pe_{\mathrm{ax,h}} = \frac{u_{\mathrm{i}}\, d_{\mathrm{p}}}{\frac{\lambda_{\mathrm{ax,g}}}{\rho_{\mathrm{f}}\, Cp_{\mathrm{f}}}} \sim 1-2 \tag{E.6}$$

$$Pe_{\mathrm{ax,h}} = \frac{u_{\mathrm{i}}\, d_{\mathrm{p}}}{\frac{\lambda_{\mathrm{ax,s}}}{\rho_{\mathrm{s}}\, Cp_{\mathrm{s}}}} \sim 1-2 \tag{E.7}$$

E.4 Heat transfer coefficient

As the adsorbent shows a spherical shape, the Heat Transfer Coefficient (HTC) in the film can be calculated with Equation E.8

$$Nu_{\mathrm{min}} = 2 = \frac{\mathrm{HTC}\, d_{\mathrm{p}}}{\lambda_{\mathrm{ax,g}}} \tag{E.8}$$

[1] Slides Engenharia das Reacções III Reaction Engineering III Integrated Master in Chemical Engineering Department of Chemical Engineering Faculty of Engineering University of Porto 2020/21, Luis Miguel Madeira.

Appendix F

Inlet and gas valve specification

F.1 Inlet specifications

The specification of the inlet flow conditions for the performed Single Component (SC) and Multi Component (MC) adsorption simulations, and the respective velocities are specified in table F.1.

Table F.1: Column's inlets specification.

Parameter		Inlet F1		Inlet F2	
		SC	MC	SC	MC
Y_{CH_4}	kmol kmol^{-1}	0.499276	0.499948	0.03	0.03
Y_{CO_2}	kmol kmol^{-1}	0.499276	0.499948	0.97	0.97
$Y_{D-Limonene}$	kmol kmol^{-1}	-	0.000428	-	0
$Y_{1-Butanol}$	kmol kmol^{-1}	-	0.000856	-	0
Y_{D4}	kmol kmol^{-1}	-	0.000058	-	0
$Y_{Toluene}$	kmol kmol^{-1}	0.00139	0.000104	0	0
F	kmol h^{-1}	70		28.2	
u_0	m s^{-1}	0.150		0.068	
T	K	298		493 (Heating) / 298 (Cooling)	
P	bar	1.4		1.4	

F.2 Gas valves' organization

When a valve is used in a system, a pressure drop is associated to the gas flow and for the performed simulations, a pressure drop of 0.2 bar across the valve was considered. In this sense, the estimation of the valves' CV value was obtained with the ratio between the flow rate and the considered pressure drop. The valves organization and specification for the three steps are represented in Table F.2

Table F.2: Valves specifications for the three stages.

	Adsorption	**Heating**	**Cooling**
VF1	$\mathrm{VF_{AS}} = 3$ $\mathrm{VF_F} = 70\ \mathrm{kmol\,h^{-1}}$	$\mathrm{VF_{AS}} = 0$	$\mathrm{VF_{AS}} = 0$
VP1	$\mathrm{VF_{AS}} = 2$ $\mathrm{VF_{CV}} = 350\ \mathrm{kmol\,h^{-1}\,bar^{-1}}$	$\mathrm{VF_{AS}} = 0$	$\mathrm{VF_{AS}} = 0$
VF2	$\mathrm{VF_{AS}} = 0$	$\mathrm{VF_{AS}} = 3$ $\mathrm{VF_F} = 28.2\ \mathrm{kmol\,h^{-1}}$	$\mathrm{VF_{AS}} = 3$ $\mathrm{VF_F} = 28.2\ \mathrm{kmol\,h^{-1}}$
VW1	$\mathrm{VF_{AS}} = 0$	$\mathrm{VF_{AS}} = 2$ $\mathrm{VF_{CV}} = 141\ \mathrm{kmol\,h^{-1}\,bar^{-1}}$	$\mathrm{VF_{AS}} = 2$ $\mathrm{VF_{CV}} = 141\ \mathrm{kmol\,h^{-1}\,bar^{-1}}$

Appendix G

Mass transfer coefficients estimation

For a first estimation of the mass transfer coefficients of each component, the following equations were considered for the calculation of the effective diffusivity (D_{h}), the pores diffusivity (D_{p}), the Knudsen diffusivity (D_{K}), the molecular diffusivity (D_{M}) and the tortuosity factor (τ).

$$D_{\mathrm{h,i}} = \frac{\varepsilon_{\mathrm{p,i}} D_{\mathrm{pi}}}{\tau} \tag{G.1}$$

$$\tau = \varepsilon_{\mathrm{p}} + 1.5(1 - \varepsilon_{\mathrm{p}}) \tag{G.2}$$

$$\frac{1}{D_{\mathrm{p,i}}} = \frac{1}{D_{\mathrm{K,i}}} + \frac{1}{D_{\mathrm{M,i}}} \tag{G.3}$$

$$D_{\mathrm{K,i}} = 0.97\ r_{\mathrm{p}} \left(\frac{T}{M_{\mathrm{W,i}}} \right)^{0.5} \tag{G.4}$$

$$D_{\mathrm{M,i}} = 1 \times 10^{2}\ T^{1.75}\ \frac{\sqrt{(M_{\mathrm{w,i}} + M_{\mathrm{w,CO_2}})\ M_{\mathrm{W,i}}\ M_{\mathrm{W,CO_2}}}}{P\left(D_{\mathrm{V,i}}^{\frac{1}{3}} + D_{\mathrm{V,CO_2}}^{\frac{1}{3}} \right)} \tag{G.5}$$

For the diffusion volume, the atomic diffusion volumes (D_{V}) were needed to take into account as the aromatic ring which is present in the toluene, which values are resumed in Table G.1. For the computation of the diffusion volume, there was a sum of all the atoms and the aromatic ring that compose each component.

Table G.1: Atomic diffusion volumes for atoms and the aromatic ring present in the compounds in study.

Component	Diffusion volume
C	15.90
H	2.31
O	6.11
Si	17.85
Aromatic Ring	-18.30

[1] Slides Engenharia das Reacções III Reaction Engineering III Integrated Master in Chemical Engineering Department of Chemical Engineering Faculty of Engineering University of Porto 2020/21, Luis Miguel Madeira.

[2] Y. Tavan, H. Azizpour, and H. Bahmanyar, "Mathematical modeling of volatile organic compounds removal over activated carbon," Journal of Environmental Chemical Engineering, vol. 9, no. 1, p. 104777, 2021.

[3] R. C. Reid, J. M. Prausnitz, and B. E. Poling, "The properties of gases and liquids"

[4] D. Ko, I. Moon, and D.-k. Choi, "Analysis of the contact time in a cyclic thermal swing adsorption process," Industrial & Engineering Chemistry Research, vol. 41, no. 6, pp. 1603–1615, 2002.

Appendix H

Settings used in the simulations

To make the simulations converge for multi-component adsorption, the tolerances of the solver options were changed, even tough there is a drawback related to the decrease in accuracy. The used settings are shown in Figure H.1. The default values for the tolerances were 1×10^{-7} and 1×10^{-5} where 1×10^{-5} and 1×10^{-4} take place in the presented figure, respectively.

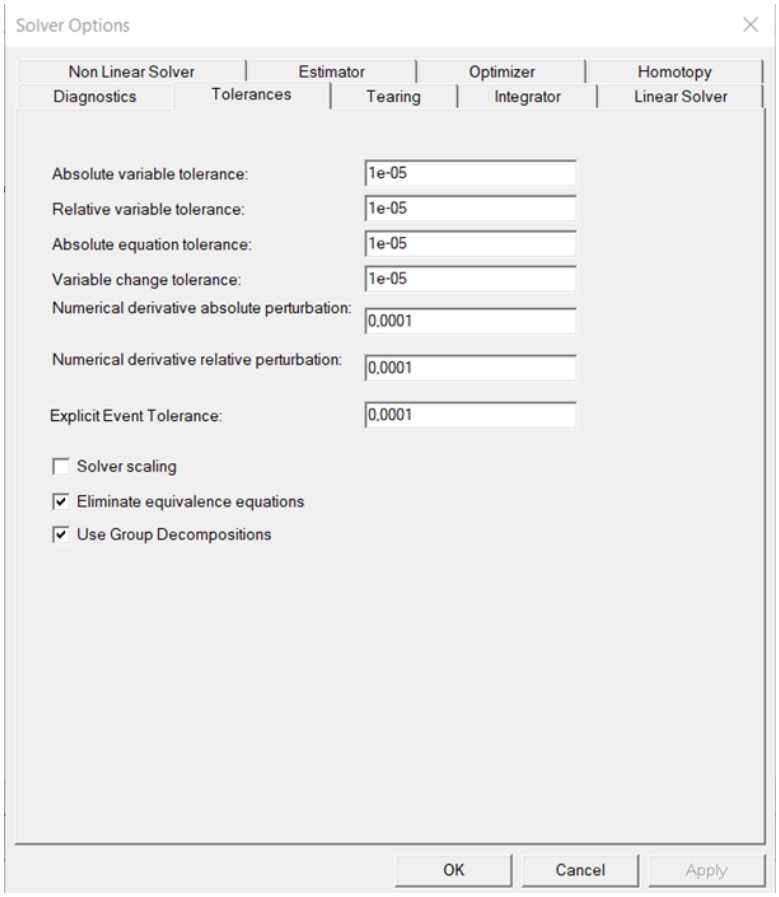

Figure H.1: Solver settings used for the performed simulations.

Appendix I

Molar fraction plots in the waste stream

Figure I.1, I.2, I.3, and I.4 represent the history of the molar fraction of the VOCs and the siloxane throughout the course of the past four cycles, for the configurations C3.1, C3.2, C2.1 and C2.2, respectively.

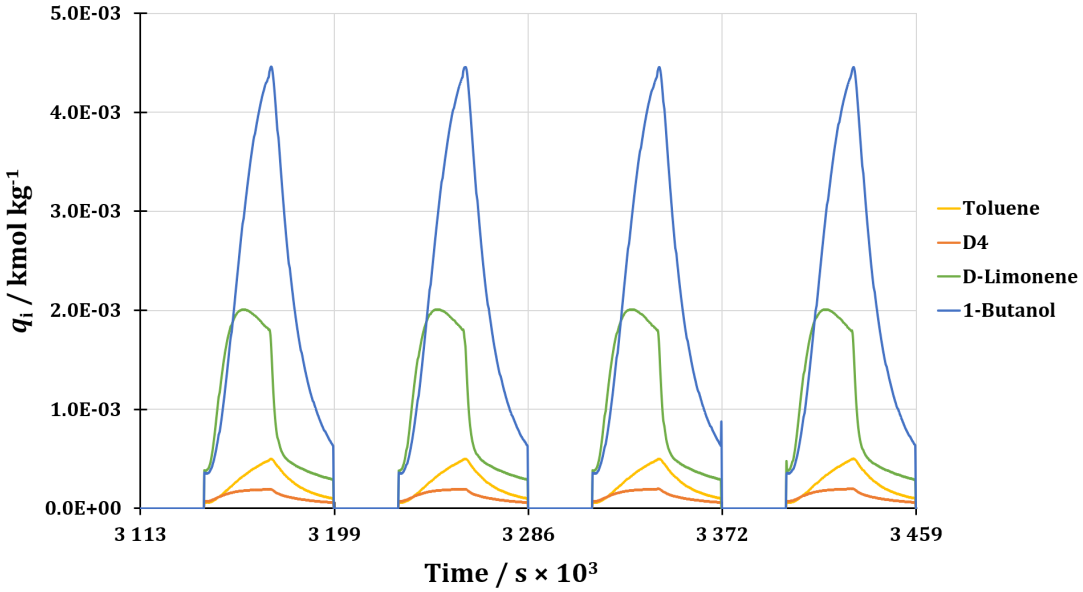

Figure I.1: Last four cycle of the components composition in the waste stream for configuration C3.1.

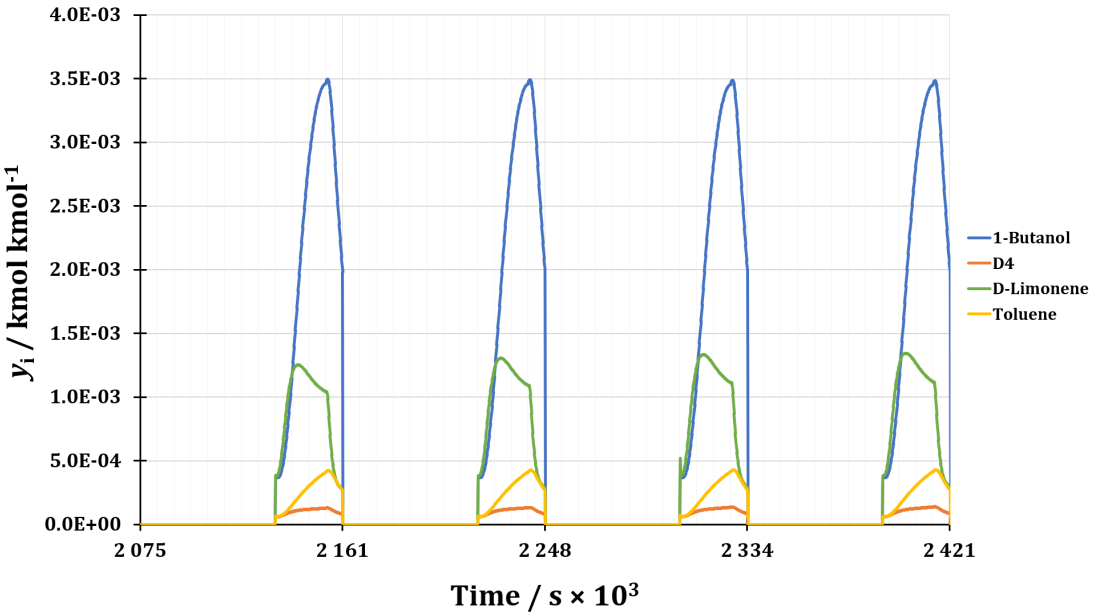

Figure I.2: Last four cycle of the components composition in the waste stream for configuration C3.2.

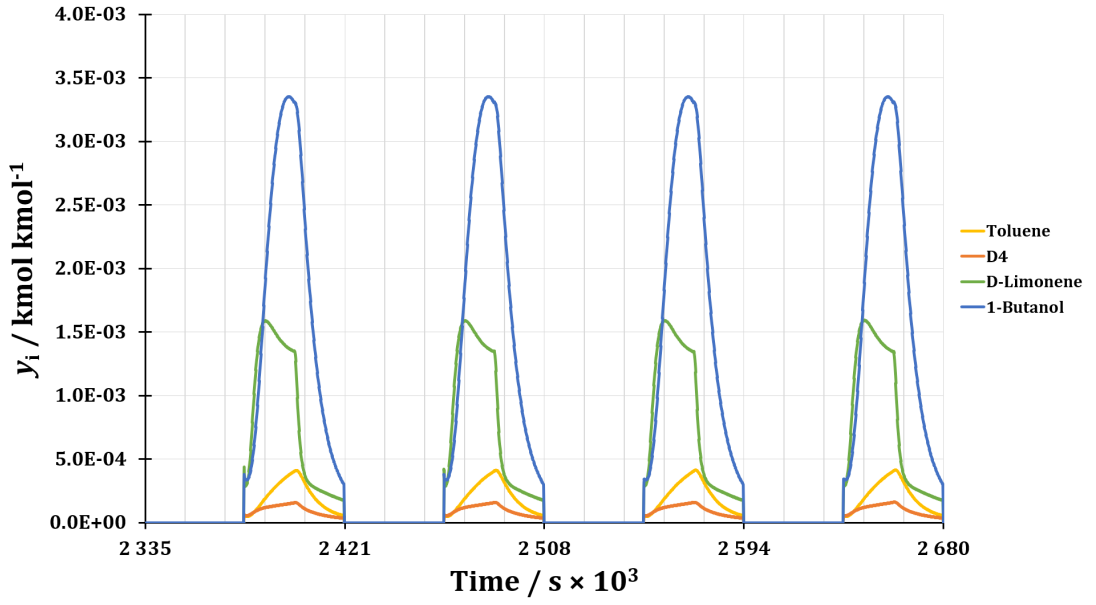

Figure I.3: Composition profile of a column from a two column configuration scheme for configuration C2.1.

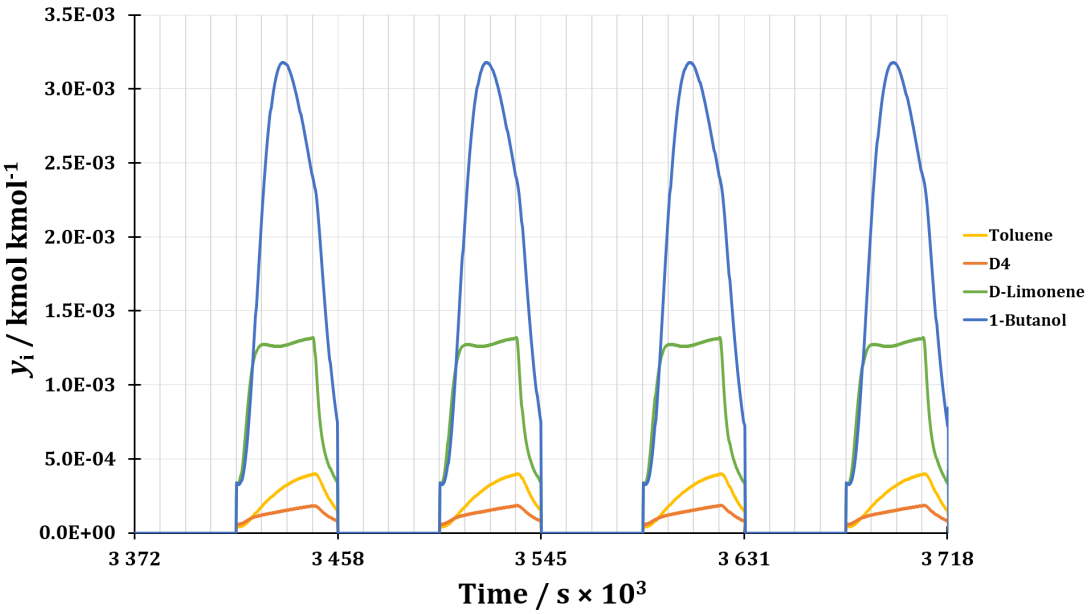

Figure I.4: Composition profile of a column from a two column alternative configuration scheme for configuration C2.2.